

---

# A Prototype-Oriented Framework for Unsupervised Domain Adaptation

---

Korawat Tanwisuth<sup>\*,1</sup>, Xinjie Fan<sup>\*,1</sup>, Huangjie Zheng<sup>\*,1</sup>, Shujian Zhang<sup>1</sup>,  
Hao Zhang<sup>2</sup>, Bo Chen<sup>3</sup>, Mingyuan Zhou<sup>1</sup>

<sup>1</sup>The University of Texas at Austin <sup>2</sup>Cornell University <sup>3</sup>Xidian University  
korawat.tanwisuth@utexas.edu, mingyuan.zhou@mcombs.utexas.edu

## Abstract

Existing methods for unsupervised domain adaptation often rely on minimizing some statistical distance between the source and target samples in the latent space. To avoid the sampling variability, class imbalance, and data-privacy concerns that often plague these methods, we instead provide a memory and computation-efficient probabilistic framework to extract class prototypes and align the target features with them. We demonstrate the general applicability of our method on a wide range of scenarios, including single-source, multi-source, class-imbalance, and source-private domain adaptation. Requiring no additional model parameters and having a moderate increase in computation over the source model alone, the proposed method achieves competitive performance with state-of-the-art methods.

## 1 Introduction

In many real-world applications, such as healthcare and autonomous driving, data labeling can be expensive and time-consuming. To make predictions on a new unlabeled dataset, one may naively use an existing supervised model trained on a large labeled dataset. However, even subtle changes in the data-collection conditions, such as lighting or background for natural images, can cause a model’s performance to degrade drastically [1]. This shift in the input data distribution is referred to in the literature as covariate shift [2]. By leveraging the labeled samples from the source domain and unlabeled samples from the target domain, unsupervised domain adaptation aims to overcome this issue, making the learned model generalize well in the target domain [3].

Ben-David et al. [4, 5] provide an  $\mathcal{H}$ -divergence based theoretical upper bound on the target error. Ganin [6] popularizes learning an invariant representation between the source and target domains to minimize this divergence. Numerous prior methods [7–12] follow this trend, focusing on using the source and target samples for feature alignment in the latent space. While this approach can reduce the discrepancy between domains, directly using the source and target samples for feature alignment has the following problems. First, several commonly used methods that can be used to quantify the difference between two empirical distributions, such as maximum mean discrepancy (MMD) [13] and Wasserstein distance [14, 15], are sensitive to outlier samples in a mini-batch when used to match the source and target marginal distributions [16, 17]. We attribute this problem to the sampling variability of both the source and target samples. Second, while we typically assume that the two domains share the same label space, we cannot guarantee that the samples drawn from the source and target domains will cover the same set of classes in each mini-batch. Especially, if the label proportions shift between domains, learning domain invariant representation might not lead

---

\* Equal contribution. Corresponding to: mingyuan.zhou@mcombs.utexas.edu  
PyTorch code is available at [https://github.com/korawat-tanwisuth/Proto\\_DA](https://github.com/korawat-tanwisuth/Proto_DA)

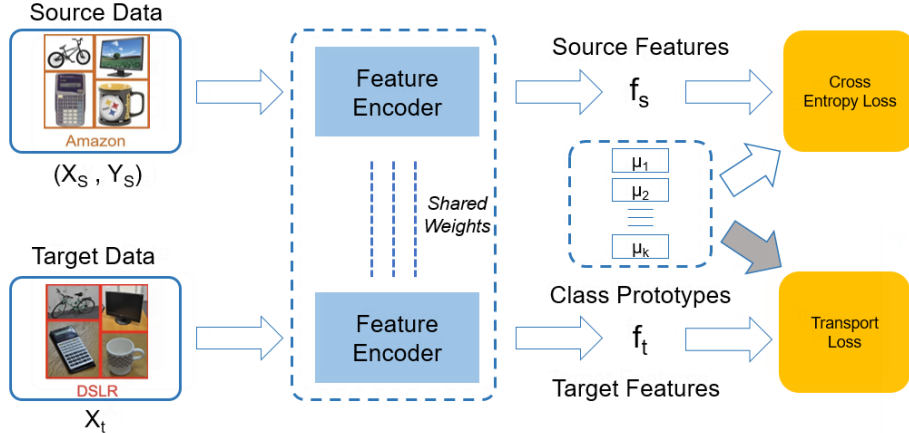


Figure 1: This figure exhibits a diagram of Prototype-oriented Conditional Transport (PCT). Unlike existing methods that align the target and source features, our method aligns the target features with class prototypes. The gray arrow indicates that the gradients of the prototypes do not back-propagate through the transport loss.

to improvements over using the source data alone to train the model [18]. If we pull the support of the source and target feature representations from different classes closer together, the classifier will be more likely to misclassify those examples. Finally, aligning the target features to source features means that we need access to both the source and target data simultaneously. In applications such as personal healthcare, we may not have access to the source data directly during the adaptation stage; instead, we may only be given access to the target data and the model trained on the source data.

We propose an algorithm that constructs class prototypes to represent the source domain samples in the latent space. Using the prototypes instead of source features avoids the previously mentioned problems: **1)** sampling variability in the source domain, **2)** instance class-mismatching in a mini-batch, and **3)** source-data privacy concerns. As we expect the classifier to make better predictions on the target data in regions where the source density is sufficiently high [19], it is natural to consider encouraging the feature encoder to map the target data close to these prototypes. Motivated by the cluster assumption [20] (decision boundaries should not cross high-density regions of the data), we provide a method to transport the target features to these class prototypes and vice versa. We further extend our bi-directional transport to address the potential shift in label proportions, a common problem that has been studied [21–25] but that has been often overlooked in prior works [6, 7, 26].

Compared to existing methods, the proposed one has several appealing aspects. First, it does not rely on adversarial training to achieve competitive performance, making the algorithm robust and converge much faster. Moreover, learnable prototypes not only avoid expensive computation but also bypass the need to directly access the source data. This attribute makes our algorithm applicable to the settings where preserving the source data privacy is a major concern. Unlike clustering-based approaches that typically require multiple forward passes before an update, our algorithm processes data in mini-batches for each update and is trained in an end-to-end manner.

We highlight the main contributions of the paper as follows: **1)** We utilize the linear classifier’s weights as class prototypes and propose a general probabilistic framework to align the target features to these prototypes. **2)** We introduce the minimization of the expected cost of a probabilistic bi-directional transport for feature alignment, and illustrate its superior performance over related methods. **3)** We test the proposed method under multiple challenging yet practical settings: single-source, multi-source, class-imbalance, and source-private domain adaptation. In comparison to state-of-the-art algorithms, the proposed prototype-oriented method achieves highly competitive performance in domain adaptation, while requiring no additional model parameters and only having a moderate increase in computation over the source model alone.

## 2 Prototype-oriented conditional transport

In this section, we propose Prototype-oriented Conditional Transport (PCT), a holistic method for domain adaption consisting of three parts: learning class prototypes, aligning the target features

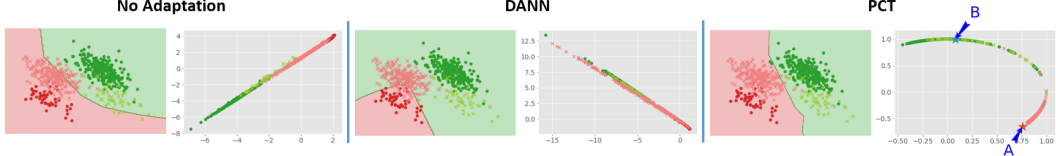


Figure 2: Visualization of different methods on a synthetic dataset, where darker points marked with “x” and lighter points marked with “.” denote the source and target samples, respectively, and the red and green colors denote two different classes. For each method, the left plot shows the data space whereas the right plot exhibits the output of the feature encoder in the latent space. Letters A and B correspond to the two class prototypes in the latent space. When there is clear class imbalance, DANN, a representative algorithm whose strategy is to match the marginal feature distributions between the source and target, fails to adapt to the target domain.

with learned prototypes using a probabilistic bi-directional transport framework of Zheng and Zhou [27], and estimating the target class proportions. Our method does not introduce additional model parameters for aligning domain features, and the model can be learned in an end-to-end manner. We provide a motivating example of the application of our method on a synthetic dataset in Figure 2.

In domain adaptation, we are given a labeled dataset from the source domain,  $\{(\mathbf{x}_i^s, y_i^s)\}_{i=1}^{n_s} \sim \mathcal{D}_s$ , and an unlabeled dataset from the target domain,  $\{\mathbf{x}_j^t\}_{j=1}^{n_t} \sim \mathcal{D}_t^x$ . We focus on the closed-category domain adaptation and assume that the source and target domains share the same label space, *i.e.*,  $y_i^s, y_j^t \in \{1, 2, \dots, K\}$ , where  $K$  denotes the number of classes. The goal of domain adaptation is to learn a model with low risk on the target samples. The model typically consists of a feature encoder,  $F_\theta: \mathcal{X} \rightarrow \mathbb{R}^{d_f}$ , parameterized by  $\theta$ , and a linear classification layer  $C_\mu: \mathbb{R}^{d_f} \rightarrow \mathbb{R}^K$ , parameterized by  $\mu$ . In prior works [6, 7, 26], the feature encoder is a pre-trained neural network, and the classifier is a randomly initialized linear layer. To simplify the following notation, we denote  $\mathbf{f}_i^s = F_\theta(\mathbf{x}_i^s)$  and  $\mathbf{f}_j^t = F_\theta(\mathbf{x}_j^t)$  as the feature representations of the source data  $\mathbf{x}_i^s$  and target data  $\mathbf{x}_j^t$ , respectively.

## 2.1 Learning class prototypes

Most existing works [6, 7, 26] focus on aligning the source and target features in a latent space. By contrast, we propose to characterize the features of each class with a class prototype and align the target features with these class prototypes instead of the source features. This approach has several advantages. First, the feature alignment between two domains would be more robust to outliers in the source domain as we avoid using the source samples directly. Second, we do not need to worry about the missing classes in the sampled mini-batch in the source domain like we do when we align the features of source and target samples. Prototypes ensure that every class is represented for each training update. Last but not least, using the inferred prototypes instead of source features allows adapting to the target domain even without accessing the source data during the adaptation stage, which is an appealing trait when preserving the source data privacy is a concern (see Table 6).

Previous methods [28–31, 12, 32] construct each class prototype as the average latent feature for that class extracted by the feature encoder, which is computationally expensive due to the forward passing of a large number of training samples. We propose to construct class prototypes in the same latent space but with learnable parameters:  $[\mu_1, \mu_2, \dots, \mu_K] \in \mathbb{R}^{d_f \times K}$ , where the dimension of each prototype,  $d_f$ , is the same as the hidden dimension after the feature encoder  $F_\theta$ . This strategy has been successfully applied by Saito et al. [33] in a semi-supervised learning setting. We learn each class prototype in a way that encourages the prototype to be close to the source samples associated with that class in the feature space. In particular, given the prototypes and source samples  $\mathbf{x}_i^s$  with features  $\mathbf{f}_i^s$  and labels  $y_i^s$ , we use the cross-entropy loss to learn the prototypes:

$$\mathcal{L}_{\text{cls}} = \mathbb{E}_{(\mathbf{x}_i^s, y_i^s) \sim \mathcal{D}_s} \left[ \sum_{k=1}^K -\log p_{ik}^s \mathbf{1}_{\{y_i^s=k\}} \right], \quad p_{ik}^s := \frac{\exp(\mu_k^T \mathbf{f}_i^s + b_k)}{\sum_{k'=1}^K \exp(\mu_{k'}^T \mathbf{f}_i^s + b_{k'})}, \quad (1)$$

where  $b_k$  is a bias term and  $p_{ik}^s$  is the predictive probability for  $\mathbf{x}_i^s$  to be classified to class  $k$ .

We note that this way of learning the class prototypes is closely connected to learning the standard linear classification layer  $C_\mu$  on source-only data with the cross-entropy loss. The neural network weights in the classification layer can be interpreted as the class prototypes. Therefore, compared with source-only approaches, constructing prototypes in this way introduce no additional parameters. As we show in Figure 4a, our method requires much fewer parameters than other domain-adaptation methods. Moreover, it requires much less computation than other prototype-based methods by avoiding the need to average the latent features for each class.

## 2.2 Bi-directional prototype-oriented conditional transport

In this section, we will discuss how we encourage the feature encoder to align the target data with class prototypes. Our approach is motivated by the cluster assumption, which has been widely adopted in both semi-supervised learning [20, 34, 35] and domain-adaptation literature [36, 37, 31, 38]. The cluster assumption states that the input data distribution consists of separated clusters and that instances belonging to the same cluster tend to have the same class labels. This means that the decision boundaries should not cross data high-density regions. To achieve this goal, we minimize the expected pairwise cost between the target features and prototypes with respect to two differently constructed joint distributions. By minimizing the expected costs under these two different joint distributions, the target feature will be close to the prototypes, far from the decision boundaries.

### 2.2.1 Moving from target domain to class prototypes

To define the expected cost of moving from the target domain to the class prototypes, we first use the chain rule to factorize the joint distribution of the class prototype  $\mu_k$  and target feature  $\mathbf{f}_j^t$  as  $p(\mathbf{f}_j^t)\pi_\theta(\mu_k | \mathbf{f}_j^t)$ , where drawing from the target feature distribution  $p(\mathbf{f}_j^t)$  can be realized by selecting a random target sample  $\mathbf{x}_j^t \sim \mathcal{D}_t^x$  to obtain  $\mathbf{f}_j^t = F_\theta(\mathbf{x}_j^t)$ . The conditional distribution, representing the probability of moving from target feature  $\mathbf{f}_j^t$  to class prototype  $\mu_k$ , is defined as

$$\pi_\theta(\mu_k | \mathbf{f}_j^t) = \frac{p(\mu_k) \exp(\mu_k^T \mathbf{f}_j^t)}{\sum_{k'=1}^K p(\mu_{k'}) \exp(\mu_{k'}^T \mathbf{f}_j^t)}, \quad k \in \{1, \dots, K\}, \quad (2)$$

where, through the lens of Bayes' rule,  $p(\mu_k)$  is the discrete prior distribution over the  $K$  classes for the target domain, and  $\exp(\mu_k^T \mathbf{f}_j^t)$  plays the role of an unnormalized likelihood term, measuring the similarity between class prototypes and target features. Intuitively, the target features are more likely to be moved to the prototypes which correspond to dominant classes in the target domain or which are closer to the target features (or both). Note that in practice we often do not have access to the target class distribution  $p(\mu_k)$ . We can use a uniform prior distribution for  $p(\mu_k)$ . However, this could be sub-optimal, especially when classes are seriously imbalanced in the target domain. To address this issue, we propose a way to estimate  $\{p(\mu_k)\}_{k=1}^K$  in Section 2.3.

We now define the expected cost of moving the target features to class prototypes as:

$$\mathcal{L}_{t \rightarrow \mu} = \mathbb{E}_{\mathbf{x}_j^t \sim \mathcal{D}_t^x} \mathbb{E}_{\mu_k \sim \pi_\theta(\mu_k | \mathbf{f}_j^t)} [c(\mu_k, \mathbf{f}_j^t)] = \mathbb{E}_{\mathbf{x}_j^t \sim \mathcal{D}_t^x} \left[ \sum_{k=1}^K c(\mu_k, \mathbf{f}_j^t) \frac{p(\mu_k) \exp(\mu_k^T \mathbf{f}_j^t)}{\sum_{k'=1}^K p(\mu_{k'}) \exp(\mu_{k'}^T \mathbf{f}_j^t)} \right], \quad (3)$$

where  $c(\cdot, \cdot)$ , a point-to-point moving cost, is defined with the cosine dissimilarity as

$$c(\mu_k, \mathbf{f}_j^t) = 1 - \frac{\mu_k^T \mathbf{f}_j^t}{\|\mu_k\|_2 \|\mathbf{f}_j^t\|_2}. \quad (4)$$

We also consider other point-to-point costs and present the results in Section 4.2. With Eq. (3), it is straightforward to obtain an unbiased estimation of  $\mathcal{L}_{t \rightarrow \mu}$  with a mini-batch from target domain  $\mathcal{D}_t^x$ .

In this target-to-prototype direction, we are assigning each target sample to the prototypes according to their similarities and the class distribution. Intuitively, minimizing this expected moving cost encourages each target feature to get closer to neighboring class prototypes, reducing the violation of the cluster assumption. If we think of each prototype as the mode of the distribution of source features for a class, this loss encourages a mode-seeking behavior [27]. Still, this loss alone might lead to sub-optimal alignment. The feature encoder can map most of the target data to only a few prototypes. We connect this loss to entropy minimization to elucidate this point.

**Connection with entropy minimization.** The expected cost of moving from the target domain to prototypes can be viewed as a generalization of entropy minimization [20], an effective regularization in many prior domain-adaptation works [39, 33, 40, 17]. If the point-to-point moving cost is defined as  $c(\mu_k, \mathbf{f}_j^t) = -\log p_{jk}^t = -\log \frac{\exp(\mu_k^T \mathbf{f}_j^t)}{\sum_{k'=1}^K \exp(\mu_{k'}^T \mathbf{f}_j^t)}$  and the conditional probability is

$$\pi_\theta(\mu_k | \mathbf{f}_j^t) = p_{jk}^t = \frac{\exp(\mu_k^T \mathbf{f}_j^t)}{\sum_{k'=1}^K \exp(\mu_{k'}^T \mathbf{f}_j^t)} \quad (\text{with a uniform prior}),$$

then the expected moving cost becomes:  $\mathcal{L}_{t \rightarrow \mu} = -\mathbb{E}_{\mathbf{x}_j^t \sim \mathcal{D}_t^x} \left[ \sum_{k=1}^K p_{jk}^t \log p_{jk}^t \right]$ , which is equivalent to minimizing the entropy on the target samples. Entropy minimization alone also has a mode-seeking behavior and has the same tendency to drop some modes (class prototypes). In other words, one trivial solution is to assign the same one-hot encoding to all the target samples [41, 42].

## 2.2.2 Moving from class prototypes to target domain

To ensure that each prototype has some target features located close by and avoid dropping class prototypes, we propose to add a cost of the opposite direction [27], *i.e.*, moving from the prototypes to target features. Given a mini-batch,  $\{\mathbf{x}_j^t\}_{j=1}^M$ , of target samples of size  $M$ , denoting  $\hat{p}(\mathbf{f}^t) = \sum_{j=1}^M \frac{1}{M} \delta_{\mathbf{f}_j^t}$  as the empirical distribution of the target features in this mini-batch, the probabilities of moving from a prototype  $\boldsymbol{\mu}_k$  to the  $M$  target features is defined as a conditional distribution:

$$\pi_{\theta}(\mathbf{f}_j^t | \boldsymbol{\mu}_k) = \frac{\hat{p}(\mathbf{f}_j^t) \exp(\boldsymbol{\mu}_k^T \mathbf{f}_j^t)}{\sum_{j'=1}^M \hat{p}(\mathbf{f}_{j'}^t) \exp(\boldsymbol{\mu}_k^T \mathbf{f}_{j'}^t)} = \frac{\exp(\boldsymbol{\mu}_k^T \mathbf{f}_j^t)}{\sum_{j'=1}^M \exp(\boldsymbol{\mu}_k^T \mathbf{f}_{j'}^t)}, \quad \mathbf{f}_j^t \in \{\mathbf{f}_1^t, \dots, \mathbf{f}_M^t\}. \quad (5)$$

As opposed to the probabilities of moving a target feature to different class prototypes  $\pi_{\theta}(\boldsymbol{\mu}_k | \mathbf{f}_j^t)$ ,  $\pi_{\theta}(\mathbf{f}_j^t | \boldsymbol{\mu}_k)$  normalizes the probabilities across the  $M$  target samples for each prototype, which ensures that each prototype will be assigned to some target features. Then, the expected cost of moving along this prototype-to-target direction is defined as:

$$\begin{aligned} \mathcal{L}_{\mu \rightarrow t} &= \mathbb{E}_{\{\mathbf{x}_j^t\}_{j=1}^M \sim \mathcal{D}_t^p} \mathbb{E}_{\boldsymbol{\mu}_k \sim p(\boldsymbol{\mu}_k)} \mathbb{E}_{\mathbf{f}_j^t \sim \pi_{\theta}(\mathbf{f}_j^t | \boldsymbol{\mu}_k)} [c(\boldsymbol{\mu}_k, \mathbf{f}_j^t)] \\ &= \mathbb{E}_{\{\mathbf{x}_j^t\}_{j=1}^M \sim \mathcal{D}_t^p} \left[ \sum_{k=1}^K p(\boldsymbol{\mu}_k) \sum_{j=1}^M c(\boldsymbol{\mu}_k, \mathbf{f}_j^t) \frac{\exp(\boldsymbol{\mu}_k^T \mathbf{f}_j^t)}{\sum_{j'=1}^M \exp(\boldsymbol{\mu}_k^T \mathbf{f}_{j'}^t)} \right], \end{aligned} \quad (6)$$

which can be estimated by drawing a mini-batch of  $M$  target samples.

Finally, combining the classification loss in Eq. (1), target-to-prototype moving cost in Eq. (3), and prototype-to-target moving cost in Eq. (6), our loss is expressed as

$$\mathcal{L}_{\text{cls}} + \mathcal{L}_{t \rightarrow \mu} + \mathcal{L}_{\mu \rightarrow t}. \quad (7)$$

Note that we treat  $\boldsymbol{\mu}$  as fixed in both  $\mathcal{L}_{t \rightarrow \mu}$  and  $\mathcal{L}_{\mu \rightarrow t}$ . This strategy allows us to apply our method in the source-data-private setting where we only have access to the source model. We also find empirically that this leads to more stable training.

## 2.3 Learning class proportions in the target domain

We propose to infer the class proportions  $\{p(\boldsymbol{\mu}_k)\}_{k=1}^K$  in the target domain by maximizing the log-likelihood of the unlabeled target data while fixing the class prototypes  $\boldsymbol{\mu}$ . Directly optimizing the marginal likelihood is intractable, so we use the EM algorithm [43–45] to derive the following iterative updates (see the derivation in Appendix B). We first initialize with a uniform prior:  $p(\boldsymbol{\mu}_k)^0 = \frac{1}{K}$ , and obtain new estimates at each update step  $l$  (starting from 0):

$$p(\boldsymbol{\mu}_k)^{l+1} = \frac{1}{M} \sum_{j=1}^M \pi_{\theta}^l(\boldsymbol{\mu}_k | \mathbf{f}_j^t), \quad \text{where } \pi_{\theta}^l(\boldsymbol{\mu}_k | \mathbf{f}_j^t) = \frac{p(\boldsymbol{\mu}_k)^l \exp(\boldsymbol{\mu}_k^T \mathbf{f}_j^t)}{\sum_{k'=1}^K p(\boldsymbol{\mu}_{k'})^l \exp(\boldsymbol{\mu}_{k'}^T \mathbf{f}_j^t)}. \quad (8)$$

Intuitively, the average predicted probabilities over the target examples for each class are used to estimate the target proportions, with  $p(\boldsymbol{\mu}_k)^{l+1}$  shown above providing an estimate based on a single mini-batch of  $M$  target samples. To estimate it based on the full dataset, we iteratively update it with  $p(\boldsymbol{\mu}_k)^{l+1} \leftarrow (1 - \beta^l) p(\boldsymbol{\mu}_k)^l + \beta^l p(\boldsymbol{\mu}_k)^{l+1}$ , where we follow the decaying schedule of the learning rate of the other parameters to set  $\beta^l = \beta_0 (1 + \gamma l)^{-\alpha}$ , in which  $\gamma = 0.0002$ ,  $\alpha = 0.75$ . The initial value  $\beta_0$  is a hyper-parameter that can be set as either 0 to indicate a uniform prior, or a small value, such as 0.001, to allow the class proportions to be inferred from the data.

## 3 Related work

**Feature distribution alignment.** Most works on domain adaptation with deep learning focus on feature alignment to align either the marginal distributions [46, 6, 8, 47, 48] or the joint distributions [7, 26] of the deep features of neural networks. Early works use adversarial-based objectives, which are equivalent to minimizing the Jensen–Shannon (JS) divergence [49]. When the source and target domains have non-overlapping supports, the JS divergence fails to supply useful gradients [50, 51]. To remedy this issue, researchers propose using the Wasserstein distance, which arises from the optimal transport problem [52]. Courty et al. [9] develop Joint Distribution Optimal Transport (JDOT), defining the transport cost to be the joint cost in the data and prediction spaces. Several works [10, 12] extend this framework for deep neural networks. However, solving for the optimal couplings without

any relaxation is a linear programming problem, which has a complexity of  $\mathcal{O}(M^3 \log M)$  [53]. Computing the transport probabilities in our algorithm has a complexity of  $\mathcal{O}(d_f MK)$ , which is the same complexity as computing the predictive probabilities that need to be computed by most algorithms. In this category, all the works focus on aligning the target features with source features, whereas we align the target features with prototypes.

**Prototype-based alignment.** We make two distinctions to existing works in this area. First, prior domain-adaptation works for classification [29–31] and segmentation [54, 55] utilize prototypes for pseudo-label assignments. By contrast, we use prototypes to behave as representative samples of the source features to define the loss. Second, all of these works use some form of average latent features to construct class prototypes, which is computationally expensive. We instead adopt a parametric approach to learn the prototypes, avoiding that costly computation.

**Learning under shifted class proportions.** Although a shift in class proportions between two domains is a common problem in many applications, it is still largely under-explored. Over the years, researchers have viewed the question through different lenses: applying kernel distribution embedding [56, 57, 21], using an EM update [43, 58], placing a meta-prior over the target proportions [59], and casting the problem under causal and anti-causal learning [21–25]. Recently, Tachet des Combes et al. [18] propose aligning the target feature distribution with a re-weighted version of the source feature distribution. While this method achieves consistent improvements over feature-alignment algorithms, it still relies on learning domain-invariant representations. As we have discussed, this approach suffers from the problems of sampling variability and class-mismatching in a mini-batch, whereas the proposed method uses class prototypes and proportion estimation to avoid these issues.

**Source-private adaptation.** Finally, the proposed method can also be applied to a source-private setting where without seeing the raw source data, we only have access to the source model and target data while adapting to the target domain [31, 47, 60–63]. Liang et al. [31] introduce a clustering-based approach to generate pseudo-labels for the target data. That approach requires constructing class centers using a weighted average of the latent features. Different from that work, our prototypes behave as class centers and are more amenable to mini-batch stochastic gradient based training.

## 4 Experiments

In this section, we evaluate our method under four practical settings: single-source, multi-source, class-imbalance, and source-private domain adaptation. We present the setup, the results, and the analysis of the results in the upcoming sections.

**Datasets.** We use the following three datasets of varying sizes in our experiment: **1) Office-31** [3] consists of 4652 images coming from three domains: Amazon (A), Webcam (W), and DSLR (D). The total number of categories is 31. **2) Office-Home** [64], a more challenging dataset than Office-31, consists of 15,500 images over 65 classes and four domains: Artistic images (Ar), Clip art (Cl), Product images (Pr), and Real-world (Rw). **3) DomainNet** [65] is a large-scale dataset for domain adaptation. It consists of about 569,010 images with 345 categories from six domains: Clipart, Infograph, Painting, Quickdraw, Real, and Sketch. We further perform experiments on Cross-Digits, ImageClef, Office-Caltech, and VisDA datasets and provide the details in Appendix E.2.

**Implementation details.** We implement our method on top of the open-source transfer learning library (MIT license) [66], adopting the default neural network architectures for both the feature encoder and linear classifier. For the feature encoder network, we utilize a pre-trained ResNet-50 in all experiments except for multi-source domain adaptation, where we use a pre-trained ResNet-101. We fine-tune the feature encoder and train the linear layers from random initialization. The linear layers have the learning rate of 0.01, 10 times that of the feature encoder. The learning rate follows the following schedule as  $\eta_{\text{iter}} = \eta_0(1 + \gamma \text{iter})^{-\alpha}$ , where  $\eta_0$  is the initial learning rate. We set  $\eta_0$  to 0.01,  $\gamma$  to 0.0002, and  $\alpha$  to 0.75. We utilize a mini-batch SGD with a momentum of 0.9. We set the batch size for the source data as  $N = 32$  and that for the target data as  $M = 96$ . We use all the labeled source samples and unlabeled target samples [6, 7, 26]. We set  $\beta_0$  to 0 (a uniform prior) in all settings except for the sub-sampled target datasets. We perform a sensitivity analysis (see Appendix E) and set  $\beta_0$  empirically to 0.001 for the sub-sampled target version of Office-31 and 0.0001 for that of Office-Home. We report the average accuracy from three independent runs. All experiments are conducted using a single Nvidia Tesla V100 GPU except for the DomainNet experiment, where we use four V100 GPUs. More implementation details can be found in Appendix D.

## 4.1 Main results

**Single-source setting.** We perform single-source domain adaptation on the Office-31 and Office-Home datasets. In each experiment, one domain serves as the source domain and another as the target domain. We consider all permutations, leading to 6 tasks for the Office-31 dataset and 12 tasks for the Office-Home dataset. We compare our algorithm with state-of-the-art algorithms for domain adaptations from three different categories: adversarial-based, divergence-based, and optimal transport-based. We report the results on Office-31 in Table 1. PCT significantly outperforms the baselines, especially on the more difficult transfer tasks (D→A and W → A). Although MDD [67], the best baseline domain-adaptation method, uses a bigger classifier, PCT still has 1.1% higher average accuracy. In Figure 4a, we visualize the number of parameters versus the average accuracy on the Office-31 dataset. While PCT uses fewer parameters than most methods, it still achieves the highest average accuracy. We report the average accuracies on the Office-Home dataset in Table 2. PCT outperforms baseline methods on 10 of the 12 transfer tasks, yielding 3.7% improvement on the average accuracy over MDD. The results in this setting demonstrate that aligning the target features with prototypes is more effective than directly aligning them with the source features.

Table 1: Accuracy (%) on Office-31 for unsupervised domain adaptation (ResNet-50).

Category	Method	A → W	D → W	W → D	A → D	D → A	W → A	Avg
	ResNet-50 [68]	68.4 ± 0.2	96.7 ± 0.1	99.3 ± 0.1	68.9 ± 0.2	62.5 ± 0.3	60.7 ± 0.3	76.1
Adversarial	DANN [6]	82.0 ± 0.4	96.9 ± 0.2	99.1 ± 0.1	79.7 ± 0.4	68.2 ± 0.4	67.4 ± 0.5	82.2
	ADDA [47]	86.2 ± 0.5	96.2 ± 0.3	98.4 ± 0.3	77.8 ± 0.3	69.5 ± 0.4	68.9 ± 0.5	82.9
	CDAN [26]	94.1 ± 0.1	98.6 ± 0.1	<b>100.0</b> ± 0.0	92.9 ± 0.2	71.0 ± 0.3	69.3 ± 0.3	87.7
	MDD [67]	94.5 ± 0.3	98.4 ± 0.1	<b>100.0</b> ± 0.0	93.5 ± 0.2	74.6 ± 0.3	72.2 ± 0.1	88.9
Divergence	JAN [7]	85.4 ± 0.3	97.4 ± 0.2	99.8 ± 0.2	84.7 ± 0.3	68.6 ± 0.3	70.0 ± 0.4	84.3
	TPN [29]	91.2 ± 0.3	97.7 ± 0.2	99.5 ± 0.1	89.9 ± 0.2	70.5 ± 0.2	73.5 ± 0.1	87.1
OT	DeepJDOT [10]	88.9 ± 0.3	98.5 ± 0.1	99.6 ± 0.2	88.2 ± 0.1	72.1 ± 0.4	70.1 ± 0.4	86.2
	ETD [69]	92.1	<b>100.0</b>	<b>100.0</b>	88.0	71.0	67.8	86.2
	PCT (Ours)	<b>94.6</b> ± 0.5	98.7 ± 0.4	99.9 ± 0.1	<b>93.8</b> ± 1.8	<b>77.2</b> ± 0.5	<b>76.0</b> ± 0.9	<b>90.0</b>

Table 2: Accuracy (%) on Office-Home for unsupervised domain adaptation (ResNet-50).

Method	Ar → Cl	Ar → Pr	Ar → Rw	Cl → Ar	Cl → Pr	Cl → Rw	Pr → Ar	Pr → Cl	Pr → Rw	Rw → Ar	Rw → Cl	Rw → Pr	Avg
ResNet-50 [68]	34.9	50.0	58.0	37.4	41.9	46.2	38.5	31.2	60.4	53.9	41.2	59.9	46.1
DANN [6]	45.6	59.3	70.1	47.0	58.5	60.9	46.1	43.7	68.5	63.2	51.8	76.8	57.6
CDAN [26]	50.7	70.6	76.0	57.6	70.0	70.0	57.4	50.9	77.3	70.9	56.7	81.6	65.8
MDD [67]	54.9	73.7	77.8	60.0	71.4	71.8	61.2	53.6	78.1	72.5	<b>60.2</b>	82.3	68.1
JAN [7]	45.9	61.2	68.9	50.4	59.7	61.0	45.8	43.4	70.3	63.9	52.4	76.8	58.3
TPN [29]	51.2	71.2	76.0	65.1	72.9	72.8	55.4	48.9	76.5	70.9	53.4	80.4	66.2
DeepJDOT [10]	48.2	69.2	74.5	58.5	69.1	71.1	56.3	46.0	76.5	68.0	52.7	80.9	64.3
ETD [69]	51.3	71.9	<b>85.7</b>	57.6	69.2	73.7	57.8	51.2	79.3	70.2	57.5	82.1	67.3
PCT (Ours)	<b>57.1</b> ± 0.3	<b>78.3</b> ± 1.2	81.4 ± 0.4	<b>67.6</b> ± 0.3	<b>77.0</b> ± 1.2	<b>76.5</b> ± 0.5	<b>68.0</b> ± 0.5	<b>55.0</b> ± 0.6	<b>81.3</b> ± 0.2	<b>74.7</b> ± 0.5	60.0 ± 0.5	<b>85.3</b> ± 0.3	<b>71.8</b>

**Multi-source setting.** In this setting, we evaluate our method using Office-Home and DomainNet datasets [65]. For each task, we select one domain as the target domain and use the remaining five domains as the source. We use the same data splitting scheme as the original paper [65]. We compare against source-combined and multi-source algorithms introduced in Venkat et al. [70] for Office-Home and in Peng et al. [65] for DomainNet. Multi-source algorithms use domain labels and a classifier for each source domain, whereas source-combined algorithms combine all the source domains into a single source domain and perform single-source adaptation. We adopt a single classifier and do not use domain labels. Thus, PCT falls under the source-combined category. We report the results in Tables 3 and 4. While PCT is not designed specifically for multi-source domain adaptation, our method still outperforms those multi-source algorithms in both datasets. Since there are more variations of the data in the source domain in this setting, the increase in performance gain verifies our intuition that prototypes help mitigate the problem of sampling variability.

Table 3: Accuracy (%) on Office-Home for ResNet50-based MSDA methods.

Category	Models	R → Ar	R → Cl	R → Pr	R → Rw	Avg
Source-combined	DAN [8]	68.5	59.4	79.0	82.5	72.4
	D-CORAL [71]	68.1	58.6	79.5	82.7	72.2
	RevGrad [6]	68.4	59.1	79.5	82.7	72.4
Multi-source	MFSAN [72]	72.1	62.0	80.3	81.8	74.1
	SlmpAI [70]	70.8	56.3	80.2	81.5	72.2
	PCT (Ours)	<b>76.3</b> ± 0.5	<b>64.1</b> ± 0.4	<b>84.9</b> ± 0.8	<b>84.3</b> ± 0.5	<b>77.4</b>

Table 4: Accuracy (%) on DomainNet for ResNet101-based MSDA methods.

Category	Models	$\mathcal{R} \rightarrow \text{Clipart}$	$\mathcal{R} \rightarrow \text{Infograph}$	$\mathcal{R} \rightarrow \text{Painting}$	$\mathcal{R} \rightarrow \text{Quickdraw}$	$\mathcal{R} \rightarrow \text{Real}$	$\mathcal{R} \rightarrow \text{Sketch}$	Avg
Multi-source	DCTN [73]	48.6 ± 0.7	23.5 ± 0.6	48.8 ± 0.6	7.2 ± 0.4	53.5 ± 0.6	47.3 ± 0.5	38.2 ± 0.6
	M <sup>3</sup> SDA [65]	57.2 ± 1.0	24.2 ± 1.2	51.6 ± 0.4	5.2 ± 0.5	61.6 ± 0.9	49.6 ± 0.6	41.5 ± 0.7
	M <sup>3</sup> SDA- $\beta$ [65]	58.6 ± 0.5	26.0 ± 0.9	52.3 ± 0.6	6.3 ± 0.6	62.7 ± 0.5	49.5 ± 0.8	42.6 ± 0.6
	ML-MSDA [74]	61.4 ± 0.8	<b>26.2 ± 0.4</b>	51.9 ± 0.2	<b>19.1 ± 0.3</b>	57.0 ± 1.0	50.3 ± 0.7	44.3 ± 0.6
Source-combined	ResNet-101 [24]	47.6 ± 0.5	13.0 ± 0.4	38.1 ± 0.5	13.3 ± 0.4	51.9 ± 0.9	33.7 ± 0.5	32.9 ± 0.5
	DAN [8]	45.4 ± 0.5	12.8 ± 0.9	36.2 ± 0.6	15.3 ± 0.4	48.6 ± 0.7	34.0 ± 0.5	32.1 ± 0.6
	RTN [75]	44.2 ± 0.6	12.6 ± 0.7	35.3 ± 0.6	14.6 ± 0.8	48.4 ± 0.7	31.7 ± 0.7	31.1 ± 0.7
	JAN [7]	40.9 ± 0.4	11.1 ± 0.6	35.4 ± 0.5	12.1 ± 0.7	45.8 ± 0.6	32.3 ± 0.6	29.6 ± 0.6
	DANN [6]	45.5 ± 0.6	13.1 ± 0.7	37.0 ± 0.7	13.2 ± 0.8	48.9 ± 0.7	31.8 ± 0.6	32.6 ± 0.7
	ADDA [47]	47.5 ± 0.8	11.4 ± 0.7	36.7 ± 0.5	14.7 ± 0.5	49.1 ± 0.8	33.5 ± 0.5	32.2 ± 0.6
	SE [38]	24.7 ± 0.3	3.9 ± 0.5	12.7 ± 0.4	7.1 ± 0.5	22.8 ± 0.5	9.1 ± 0.5	16.1 ± 0.4
	MCD [76]	54.3 ± 0.6	22.1 ± 0.7	45.7 ± 0.6	7.6 ± 0.5	58.4 ± 0.7	43.5 ± 0.6	38.5 ± 0.6
	PCT (Ours)	<b>67.2 ± 0.5</b>	26.1 ± 0.2	<b>55.0 ± 0.2</b>	16.2 ± 0.2	<b>67.1 ± 0.2</b>	<b>53.7 ± 0.6</b>	<b>47.6 ± 0.1</b>

**Sub-sampled setting.** In many cases, the label proportions could significantly change from one dataset to another, resulting in a decrease in a model’s performance. To test our algorithm under this setting, we follow the experimental protocol in Tachet des Combes et al. [18]. We keep only thirty percent of the first  $\lfloor K/2 \rfloor$  classes to simulate class imbalance. We directly take their results for the sub-sampled source data and perform additional experiments using the same sub-sampling scheme on the target data. The baselines in this setting are standard domain adaptation methods (DAN, JAN, and CDAN) and their importance weighted versions introduced in Tachet des Combes et al. [18]. We present the results in Table 5. On the sub-sampled source data, PCT with uniform prior outperforms the second-best method (IWCDAN) by 4% on Office-31 and 6.6% on Office-Home. Learning the prior distribution on the target domain does not improve the result, as this setting does not have a serious imbalance issue in the target domain. On the sub-sampled target data, PCT with a uniform prior already outperforms the baselines, 1.9% and 5.2% higher average accuracy than IWCDAN’s on Office-31 and Office-Home, respectively. Using a learnable prior further improves upon using a uniform prior by 1.0% on Office-31 and by 0.4% on Office-Home. The improvements confirm our intuition that prototypes help with the class imbalance in both the source and target domain while estimating the target proportion further boosts the performance in the target domain sub-sampled setting. We visualize the estimated proportions on the target data in Figure 3, verifying that the proportions are inferred correctly.

Table 5: Average accuracy (%) on sub-sampled version of Office-31 and Office-Home (ResNet-50).

Method	sub-S O-31	sub-T O-31	sub-S O-H	sub-T O-H
ResNet-50 [68]	75.7	76.1	51.4	58.2
DANN [8]	76.2	75.9	51.8	58.3
JAN [7]	78.2	78.1	53.9	61.4
CDAN [26]	81.6	83.0	56.3	63.1
IWDAN [18]	82.6	79.2	57.6	58.6
IWJAN [18]	82.6	82.8	55.9	62.0
IWCDAN [18]	83.9	83.5	61.2	64.6
PCT-Uniform (Ours)	<b>87.9 ± 0.4</b>	85.4 ± 0.3	<b>67.8 ± 0.3</b>	69.8 ± 0.2
PCT-Learnable (Ours)	<b>87.9 ± 0.4</b>	<b>86.4 ± 0.2</b>	<b>67.8 ± 0.3</b>	<b>70.2 ± 0.2</b>

**Source-data-private setting.** In many practical applications, practitioners might not directly have access to the source data in the adaptation stage. Instead, a trained model on the source data is provided. In this setting, the goal is to adapt to the target domain while only operating on the given model. We compare our method with Source Hypothesis Transfer (SHOT) [31], a state-of-the-art method proposed specifically for this setting. SHOT contains two losses: an information maximization (IM) loss and a pseudo-labeling loss. We follow their experimental protocol by first training the model on the source data alone. During the adaptation stage, we only use the target data to perform model adaptation. We use the transport losses to update the feature encoder while fixing the prototypes. We report the results in Table 6. From the standard setting where we have access to source data in Table 1, the average accuracy drops by 1.6% for Office-31 and by 0.8% for Office-Home. On the Office-31 dataset, our bi-directional loss outperforms the IM loss by 1.1% and the pseudo label loss by 0.8%. While the average accuracy for our method is 0.2% lower than both of their losses combined, the  $p$ -value for the independent two-sample  $t$ -test on the accuracies of different runs is 0.32, which is not statistically significant. On the Office-Home dataset, our approach performs 1.9% and 0.5% better than the pseudo label and IM losses, respectively. While their combined loss achieves 0.8% accuracy higher than that of our method, the pseudo-labeling loss in SHOT requires



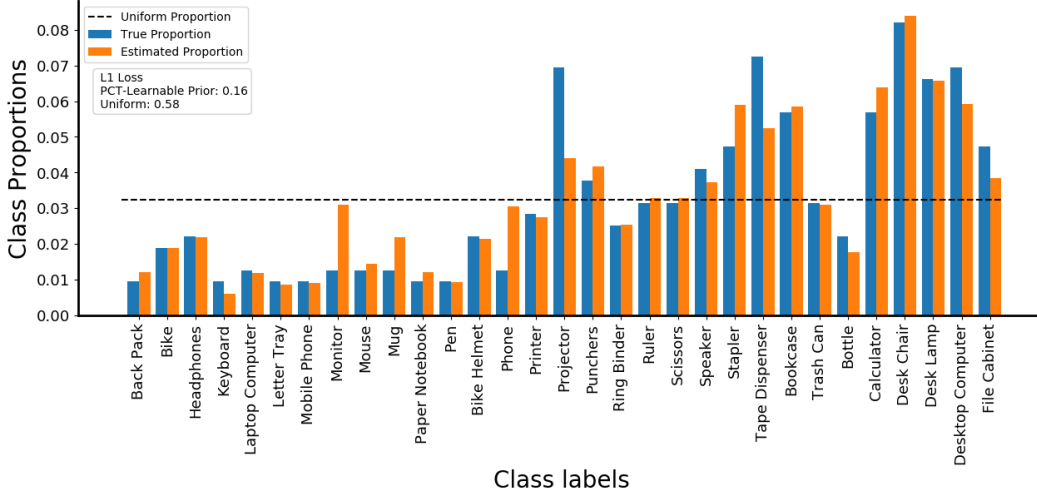


Figure 3: Visualization of the estimated target proportions versus true class proportions for the task  $A \rightarrow sD$  on the Office-31 dataset. The dotted line represents a uniform proportion. It is clear that each orange bar (the learned proportions) is close to its adjacent blue bar (the true proportion). To quantify this observation, we measure the L1 loss between the true and learned proportions. The estimated proportions achieve lower L1 loss than the uniform distribution (0.16 vs 0.58), illustrating the effectiveness of our estimation strategy.

Table 6: Average Accuracy (%) on the source-private Office-31 and Office-Home (ResNet-50).

	Source Model Only	SHOT-Pseudo Label [31]	SHOT-IM [31]	SHOT [31]	PCT (Ours)
Office-31	79.3	87.6 $\pm$ 0.5	87.3 $\pm$ 0.5	<b>88.6 <math>\pm</math> 0.4</b>	88.4 $\pm$ 0.6
Office-Home	60.2	69.1 $\pm$ 0.6	70.5 $\pm$ 0.3	<b>71.8 <math>\pm</math> 0.4</b>	71.0 $\pm$ 0.6

constructing class centers, which does not scale well with large datasets. Our approach uses the classifier’s weights as class prototypes to avoid this issue.

## 4.2 Analysis of results

**Ablation study.** To examine the effect of each component in our framework, we perform ablation studies and present the results in Table 7. **1) Alignment strategy.** Next, we present the result using optimal transport as the alignment strategy. We consider two variants of Prototype-oriented Optimal Transport (POT): exact linear program (POT) and Sinkhorn relaxation (POT-Sinkhorn). In each variant, we solve for the optimal couplings using the optimal transport formulation. After obtaining the transport probabilities, we update the feature encoder using the obtained probabilities as the weights for the transport cost. We can see that POT performs 1.7% better than DeepJDOT in Table 1, showing the effectiveness of using prototypes to define the transport costs with the target features. Still, both versions of POT underperforms PCT by 2.1% and 1.7%, respectively. **2) Effect of each loss in PCT.** We examine the effect of each loss on the average test accuracy on the Office-31 dataset. We remove each transport loss while keeping the cross-entropy loss. The bi-directional loss leads to the best accuracy, while the drop in accuracy is more significant if we remove  $\mathcal{L}_{\mu \rightarrow t}$ . This result is not surprising because, without  $\mathcal{L}_{\mu \rightarrow t}$ , the model can map target data to only a few prototypes, leading to a degenerate solution. **3) Gradient stopping.** We also show the algorithm’s performance without stopping the gradient of  $\mu$  in the transport loss. PCT gains an additional 1.0% in accuracy with the gradient stopping strategy. The performance gain is consistent with the finding in recent work by Chen and He [77], where the authors apply the gradient stopping strategy to avoid degenerate solutions in contrastive learning. **4) Cost function.** Finally, we explore the cost function inspired by the radial basis kernel. We can see that the cosine distance in PCT gives 3.1% higher average accuracy. In short, the choice of the probabilistic bi-directional transport framework, gradient-stopping strategy, and point-to-point cost function all contribute to the success of the proposed PCT method.

Table 7: Average accuracy (%) of PCT on Office-31 under different variants (ResNet-50).

POT	POT-Sinkhorn	PCT w/o ( $\mathcal{L}_{t \rightarrow \mu}$ )	PCT w/o ( $\mathcal{L}_{\mu \rightarrow t}$ )	w/o stop-grad	$c(\mu_k, \mathbf{f}_j^t) = \exp(-\mu_k^T \mathbf{f}_j^t)$	PCT (Ours)
87.9 $\pm$ 0.8	88.3 $\pm$ 0.9	88.6 $\pm$ 0.2	84.3 $\pm$ 0.9	89.0 $\pm$ 0.3	86.9 $\pm$ 0.4	90.0 $\pm$ 0.5

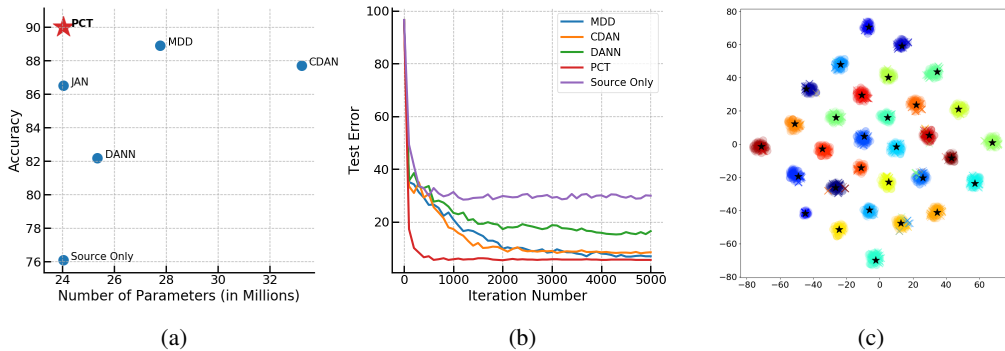


Figure 4: (a) Analysis of parameter efficiency, (b) comparison of convergence, and (c) a t-SNE visualization of the output of the feature encoder trained with PCT on the task  $A \rightarrow W$ . In plot (c), prototypes ( $\star$ ), source features ( $\cdot$ ), and target features ( $\times$ ) are tightly clustered together for each class.

**Convergence comparison.** We plot test accuracy versus iteration number on the task ( $A \rightarrow W$ ) in Figure 4b to compare the convergence rate of different algorithms. We also visualize test accuracy versus convergence time in minutes in Appendix E. In both plots, PCT quickly converges within the first one thousand iterations, and the test accuracy does not fluctuate much thereafter. This phenomenon is not surprising since we use prototypes instead of the source features to align with the target features. We expect the prototypes to behave as representative samples of the source features, making the model converge quickly and stably.

**Visualization.** We visualize in Figure 4c the t-SNE plot of the source and target features as well as the prototypes for the task  $A \rightarrow W$ . Figure 4c shows that both the source (dots  $\cdot$ ) and target (crosses  $\times$ ) features are close to the prototypes (black stars  $\star$ ), indicating that our algorithm is learning meaningful prototypes and successfully align the target features with the prototypes.

## 5 Conclusion

We offer a holistic framework for unsupervised domain adaptation through the lens of a probabilistic bi-directional transport between the target features and class prototypes. With extensive experiments under various application scenarios of unsupervised domain adaptation, we show that the proposed prototype-oriented alignment method works well on multiple datasets, is robust against class imbalance, and can perform domain adaptation with no direct access to the source data. Without adding additional model parameters, our memory and computation-efficient algorithm achieves competitive performance with state-of-the-art methods on several widely used benchmarks.

## Acknowledgments

We thank Camillia Smith Barnes and Georgii Riabov for helpful discussions and feedback on the paper. K. Tanwisuth, X. Fan, H. Zheng, S. Zhang, and M. Zhou acknowledge the support of Grant IIS-1812699 from the U.S. National Science Foundation, the APX 2019 project sponsored by the Office of the Vice President for Research at The University of Texas at Austin, the support of a gift fund from ByteDance Inc., and the Texas Advanced Computing Center (TACC) for providing HPC resources that have contributed to the research results reported within this paper.

## References

- [1] Ali Farhadi and Mostafa Kamali Tabrizi. Learning to recognize activities from the wrong view point. In *European conference on computer vision*, pages 154–166. Springer, 2008.
- [2] Hidetoshi Shimodaira. Improving predictive inference under covariate shift by weighting the log-likelihood function. *Journal of statistical planning and inference*, 90(2):227–244, 2000.
- [3] Kate Saenko, Brian Kulis, Mario Fritz, and Trevor Darrell. Adapting visual category models to new domains. In *European conference on computer vision*, pages 213–226. Springer, 2010.
- [4] Shai Ben-David, John Blitzer, Koby Crammer, and Fernando Pereira. Analysis of representations for domain adaptation. In B. Schölkopf, J. Platt, and T. Hoffman, editors, *Advances in Neural Information Processing Systems*, volume 19. MIT Press, 2007.
- [5] Shai Ben-David, John Blitzer, Koby Crammer, Alex Kulesza, Fernando Pereira, and Jennifer Vaughan. A theory of learning from different domains. *Machine Learning*, 79:151–175, 2010.
- [6] Yaroslav Ganin and Victor S. Lempitsky. Unsupervised domain adaptation by backpropagation. In Francis R. Bach and David M. Blei, editors, *ICML*, volume 37 of *JMLR Workshop and Conference Proceedings*, pages 1180–1189. JMLR.org, 2015.
- [7] Mingsheng Long, Han Zhu, Jianmin Wang, and Michael I. Jordan. Deep transfer learning with joint adaptation networks. In Doina Precup and Yee Whye Teh, editors, *Proceedings of the 34th International Conference on Machine Learning*, volume 70 of *Proceedings of Machine Learning Research*, pages 2208–2217. PMLR, 06–11 Aug 2017.
- [8] Mingsheng Long, Yue Cao, Jianmin Wang, and Michael I. Jordan. Learning transferable features with deep adaptation networks. In *Proceedings of the 32nd International Conference on Machine Learning, ICML 2015, Lille, France, 6-11 July 2015*, pages 97–105, 2015.
- [9] Nicolas Courty, Rémi Flamary, Amaury Habrard, and Alain Rakotomamonjy. Joint distribution optimal transportation for domain adaptation. In I. Guyon, U. V. Luxburg, S. Bengio, H. Wallach, R. Fergus, S. Vishwanathan, and R. Garnett, editors, *Advances in Neural Information Processing Systems*, volume 30. Curran Associates, Inc., 2017.
- [10] Bharath Bhushan Damodaran, Benjamin Kellenberger, Rémi Flamary, Devis Tuia, and Nicolas Courty. DeepJDOT: Deep joint distribution optimal transport for unsupervised domain adaptation. *CoRR*, abs/1803.10081, 2018.
- [11] Chen-Yu Lee, Tanmay Batra, Mohammad Haris Baig, and Daniel Ulbricht. Sliced Wasserstein discrepancy for unsupervised domain adaptation. In *Proceedings of the IEEE/CVF Conference on Computer Vision and Pattern Recognition*, pages 10285–10295, 2019.
- [12] Renjun Xu, Pelen Liu, Liyan Wang, Chao Chen, and Jindong Wang. Reliable weighted optimal transport for unsupervised domain adaptation. In *Proceedings of the IEEE/CVF Conference on Computer Vision and Pattern Recognition (CVPR)*, June 2020.
- [13] Arthur Gretton, Karsten M Borgwardt, Malte J Rasch, Bernhard Schölkopf, and Alexander Smola. A kernel two-sample test. *The Journal of Machine Learning Research*, 13(1):723–773, 2012.
- [14] Leonid V Kantorovich. On the translocation of masses. *Journal of Mathematical Sciences*, 133(4):1381–1382, 2006.
- [15] Gabriel Peyré and Marco Cuturi. Computational optimal transport. *Foundations and Trends in Machine Learning*, 11(5-6):355–607, 2019.
- [16] Matthieu Lerasle, Zoltán Szabó, Timothée Mathieu, and Guillaume Lecué. Monk outlier-robust mean embedding estimation by median-of-means. In *International Conference on Machine Learning*, pages 3782–3793. PMLR, 2019.
- [17] Yogesh Balaji, Rama Chellappa, and Soheil Feizi. Robust optimal transport with applications in generative modeling and domain adaptation. In *Advances in Neural Information Processing Systems*, 2020.

- [18] Remi Tachet des Combes, Han Zhao, Yu-Xiang Wang, and Geoff Gordon. Domain adaptation with conditional distribution matching and generalized label shift. In *Advances in Neural Information Processing Systems*, 2020.
- [19] Fredrik D. Johansson, David Sontag, and Rajesh Ranganath. Support and invertibility in domain-invariant representations. In Kamalika Chaudhuri and Masashi Sugiyama, editors, *Proceedings of Machine Learning Research*, volume 89 of *Proceedings of Machine Learning Research*, pages 527–536, 16–18 Apr 2019.
- [20] Yves Grandvalet, Yoshua Bengio, et al. Semi-supervised learning by entropy minimization. In *CAP*, pages 281–296, 2005.
- [21] Kun Zhang, Bernhard Schölkopf, Krikamol Muandet, and Zhikun Wang. Domain adaptation under target and conditional shift. In *International Conference on Machine Learning*, pages 819–827. PMLR, 2013.
- [22] Bernhard Schölkopf, Dominik Janzing, Jonas Peters, Eleni Sgouritsa, Kun Zhang, and Joris Mooij. On causal and anticausal learning. *arXiv preprint arXiv:1206.6471*, 2012.
- [23] Mingming Gong, Kun Zhang, Tongliang Liu, Dacheng Tao, Clark Glymour, and Bernhard Schölkopf. Domain adaptation with conditional transferable components. In *International conference on machine learning*, pages 2839–2848. PMLR, 2016.
- [24] Zachary Lipton, Yu-Xiang Wang, and Alexander Smola. Detecting and correcting for label shift with black box predictors. In *International conference on machine learning*, pages 3122–3130. PMLR, 2018.
- [25] Kamyar Azizzadenesheli, Anqi Liu, Fanny Yang, and Animashree Anandkumar. Regularized learning for domain adaptation under label shifts. *arXiv preprint arXiv:1903.09734*, 2019.
- [26] Mingsheng Long, Zhangjie Cao, Jianmin Wang, and Michael I Jordan. Conditional adversarial domain adaptation. In S. Bengio, H. Wallach, H. Larochelle, K. Grauman, N. Cesa-Bianchi, and R. Garnett, editors, *Advances in Neural Information Processing Systems*, volume 31. Curran Associates, Inc., 2018.
- [27] Huangjie Zheng and Mingyuan Zhou. Comparing probability distributions with conditional transport. *arXiv preprint arXiv:2012.14100*, 2020.
- [28] Jake Snell, Kevin Swersky, and Richard Zemel. Prototypical networks for few-shot learning. In *Proceedings of the 31st International Conference on Neural Information Processing Systems*, pages 4080–4090, 2017.
- [29] Yingwei Pan, Ting Yao, Yehao Li, Yu Wang, Chong-Wah Ngo, and Tao Mei. Transferrable prototypical networks for unsupervised domain adaptation. In *Proceedings of the IEEE/CVF Conference on Computer Vision and Pattern Recognition (CVPR)*, 2019.
- [30] Guoliang Kang, Lu Jiang, Yi Yang, and Alexander G Hauptmann. Contrastive adaptation network for unsupervised domain adaptation. In *Proceedings of the IEEE/CVF Conference on Computer Vision and Pattern Recognition*, pages 4893–4902, 2019.
- [31] Jian Liang, Dapeng Hu, and Jiashi Feng. Do we really need to access the source data? source hypothesis transfer for unsupervised domain adaptation. In *International Conference on Machine Learning*, pages 6028–6039. PMLR, 2020.
- [32] Xiangyu Yue, Zangwei Zheng, Shanghang Zhang, Yang Gao, Trevor Darrell, Kurt Keutzer, and Alberto Sangiovanni Vincentelli. Prototypical cross-domain self-supervised learning for few-shot unsupervised domain adaptation. In *Proceedings of the IEEE/CVF Conference on Computer Vision and Pattern Recognition*, pages 13834–13844, 2021.
- [33] Kuniaki Saito, Donghyun Kim, Stan Sclaroff, Trevor Darrell, and Kate Saenko. Semi-supervised domain adaptation via minimax entropy. In *Proceedings of the IEEE/CVF International Conference on Computer Vision*, pages 8050–8058, 2019.

- [34] Takeru Miyato, Shin-ichi Maeda, Masanori Koyama, and Shin Ishii. Virtual adversarial training: a regularization method for supervised and semi-supervised learning. *IEEE transactions on pattern analysis and machine intelligence*, 41(8):1979–1993, 2018.
- [35] Samuli Laine and Timo Aila. Temporal ensembling for semi-supervised learning. *arXiv preprint arXiv:1610.02242*, 2016.
- [36] Yuan Shi and Fei Sha. Information-theoretical learning of discriminative clusters for unsupervised domain adaptation. *arXiv preprint arXiv:1206.6438*, 2012.
- [37] Rui Shu, Hung H Bui, Hirokazu Narui, and Stefano Ermon. A dirt-t approach to unsupervised domain adaptation. *arXiv preprint arXiv:1802.08735*, 2018.
- [38] Geoffrey French, Michal Mackiewicz, and Mark Fisher. Self-ensembling for visual domain adaptation. *arXiv preprint arXiv:1706.05208*, 2017.
- [39] Tuan-Hung Vu, Himalaya Jain, Maxime Bucher, Matthieu Cord, and Patrick Pérez. Advent: Adversarial entropy minimization for domain adaptation in semantic segmentation. In *Proceedings of the IEEE/CVF Conference on Computer Vision and Pattern Recognition*, pages 2517–2526, 2019.
- [40] Kuniaki Saito, Donghyun Kim, Stan Sclaroff, and Kate Saenko. Universal domain adaptation through self supervision. *arXiv preprint arXiv:2002.07953*, 2020.
- [41] Pietro Morerio, Jacopo Cavazza, and Vittorio Murino. Minimal-entropy correlation alignment for unsupervised deep domain adaptation. *arXiv preprint arXiv:1711.10288*, 2017.
- [42] Xiaofu Wu, Quan Zhou, Zhen Yang, Chunming Zhao, Longin Jan Latecki, et al. Entropy minimization vs. diversity maximization for domain adaptation. *arXiv preprint arXiv:2002.01690*, 2020.
- [43] Marco Saerens, Patrice Latinne, and Christine Decaestecker. Adjusting the outputs of a classifier to new a priori probabilities: a simple procedure. *Neural computation*, 14(1):21–41, 2002.
- [44] Guoliang Kang, Liang Zheng, Yan Yan, and Yi Yang. Deep adversarial attention alignment for unsupervised domain adaptation: the benefit of target expectation maximization. In *Proceedings of the European Conference on Computer Vision (ECCV)*, pages 401–416, 2018.
- [45] Amr Alexandari, Anshul Kundaje, and Avanti Shrikumar. Maximum likelihood with bias-corrected calibration is hard-to-beat at label shift adaptation. In *International Conference on Machine Learning*, pages 222–232. PMLR, 2020.
- [46] Eric Tzeng, Judy Hoffman, Ning Zhang, Kate Saenko, and Trevor Darrell. Deep domain confusion: Maximizing for domain invariance. *arXiv preprint arXiv:1412.3474*, 2014.
- [47] Eric Tzeng, Judy Hoffman, Kate Saenko, and Trevor Darrell. Adversarial discriminative domain adaptation. In *Proceedings of the IEEE conference on computer vision and pattern recognition*, pages 7167–7176, 2017.
- [48] Shujian Zhang, Xinjie Fan, Huangjie Zheng, Korawat Tanwisuth, and Mingyuan Zhou. Alignment attention by matching key and query distributions. In *NeurIPS 2021: Neural Information Processing Systems*, Dec. 2021.
- [49] Ian J Goodfellow, Jean Pouget-Abadie, Mehdi Mirza, Bing Xu, David Warde-Farley, Sherjil Ozair, Aaron Courville, and Yoshua Bengio. Generative adversarial networks. *arXiv preprint arXiv:1406.2661*, 2014.
- [50] Martin Arjovsky, Soumith Chintala, and Léon Bottou. Wasserstein generative adversarial networks. In *International conference on machine learning*, pages 214–223. PMLR, 2017.
- [51] Soheil Kolouri, Phillip E Pope, Charles E Martin, and Gustavo K Rohde. Sliced Wasserstein auto-encoders. In *International Conference on Learning Representations*, 2018.
- [52] Cédric Villani. *Optimal transport: old and new*, volume 338. Springer Science & Business Media, 2008.

- [53] Quentin Mérigot and Edouard Oudet. Discrete optimal transport: complexity, geometry and applications. *Discrete & Computational Geometry*, 55(2):263–283, 2016.
- [54] Qiming Zhang, Jing Zhang, Wei Liu, and Dacheng Tao. Category anchor-guided unsupervised domain adaptation for semantic segmentation. *arXiv preprint arXiv:1910.13049*, 2019.
- [55] Shaoan Xie, Zibin Zheng, Liang Chen, and Chuan Chen. Learning semantic representations for unsupervised domain adaptation. In *International conference on machine learning*, pages 5423–5432. PMLR, 2018.
- [56] Marthinus Christoffel Du Plessis and Masashi Sugiyama. Semi-supervised learning of class balance under class-prior change by distribution matching. *Neural Networks*, 50:110–119, 2014.
- [57] Tuan Duong Nguyen, Marthinus Christoffel, and Masashi Sugiyama. Continuous target shift adaptation in supervised learning. In *Asian Conference on Machine Learning*, pages 285–300. PMLR, 2016.
- [58] Yee Seng Chan and Hwee Tou Ng. Word sense disambiguation with distribution estimation. In *IJCAI*, volume 5, pages 1010–5. Citeseer, 2005.
- [59] Amos Storkey. When training and test sets are different: Characterizing learning transfer. *Dataset shift in machine learning*, 30:3–28, 2009.
- [60] Rui Li, Qianfen Jiao, Wenming Cao, Hau-San Wong, and Si Wu. Model adaptation: Unsupervised domain adaptation without source data. In *Proceedings of the IEEE/CVF Conference on Computer Vision and Pattern Recognition*, pages 9641–9650, 2020.
- [61] Vinod K Kurmi, Venkatesh K Subramanian, and Vinay P Namboodiri. Domain impression: A source data free domain adaptation method. In *Proceedings of the IEEE/CVF Winter Conference on Applications of Computer Vision*, pages 615–625, 2021.
- [62] Jogendra Nath Kundu, Rahul Mysore Venkatesh, Naveen Venkat, Ambareesh Revanur, and R Venkatesh Babu. Class-incremental domain adaptation. In *Computer Vision–ECCV 2020: 16th European Conference, Glasgow, UK, August 23–28, 2020, Proceedings, Part XIII 16*, pages 53–69. Springer, 2020.
- [63] Jogendra Nath Kundu, Naveen Venkat, R Venkatesh Babu, et al. Universal source-free domain adaptation. In *Proceedings of the IEEE/CVF Conference on Computer Vision and Pattern Recognition*, pages 4544–4553, 2020.
- [64] Hemanth Venkateswara, Jose Eusebio, Shayok Chakraborty, and Sethuraman Panchanathan. Deep hashing network for unsupervised domain adaptation. In *Proceedings of the IEEE conference on computer vision and pattern recognition*, pages 5018–5027, 2017.
- [65] Xingchao Peng, Qinxun Bai, Xide Xia, Zijun Huang, Kate Saenko, and Bo Wang. Moment matching for multi-source domain adaptation. In *Proceedings of the IEEE/CVF International Conference on Computer Vision*, pages 1406–1415, 2019.
- [66] Mingsheng Long Janguang Jiang, Bo Fu. Transfer-learning-library. <https://github.com/thuml/Transfer-Learning-Library>, 2020.
- [67] Yuchen Zhang, Tianle Liu, Mingsheng Long, and Michael Jordan. Bridging theory and algorithm for domain adaptation. In *International Conference on Machine Learning*, pages 7404–7413. PMLR, 2019.
- [68] Kaiming He, Xiangyu Zhang, Shaoqing Ren, and Jian Sun. Deep residual learning for image recognition. In *Proceedings of the IEEE conference on computer vision and pattern recognition*, pages 770–778, 2016.
- [69] Mengxue Li, Yi-Ming Zhai, You-Wei Luo, Peng-Fei Ge, and Chuan-Xian Ren. Enhanced transport distance for unsupervised domain adaptation. In *Proceedings of the IEEE/CVF Conference on Computer Vision and Pattern Recognition*, pages 13936–13944, 2020.

- [70] Naveen Venkat, Jogendra Nath Kundu, Durgesh Kumar Singh, Ambareesh Revanur, and R Venkatesh Babu. Your classifier can secretly suffice multi-source domain adaptation. *arXiv preprint arXiv:2103.11169*, 2021.
- [71] Baochen Sun and Kate Saenko. Deep coral: Correlation alignment for deep domain adaptation. In *European conference on computer vision*, pages 443–450. Springer, 2016.
- [72] Yongchun Zhu, Fuzhen Zhuang, and Deqing Wang. Aligning domain-specific distribution and classifier for cross-domain classification from multiple sources. In *Proceedings of the AAAI Conference on Artificial Intelligence*, volume 33, pages 5989–5996, 2019.
- [73] Ruijia Xu, Ziliang Chen, Wangmeng Zuo, Junjie Yan, and Liang Lin. Deep cocktail network: Multi-source unsupervised domain adaptation with category shift. In *Proceedings of the IEEE Conference on Computer Vision and Pattern Recognition*, pages 3964–3973, 2018.
- [74] Zhenpeng Li, Zhen Zhao, Yuhong Guo, Haifeng Shen, and Jieping Ye. Mutual learning network for multi-source domain adaptation. *arXiv preprint arXiv:2003.12944*, 2020.
- [75] Mingsheng Long, Han Zhu, Jianmin Wang, and Michael I Jordan. Unsupervised domain adaptation with residual transfer networks. *arXiv preprint arXiv:1602.04433*, 2016.
- [76] Kuniaki Saito, Kohei Watanabe, Yoshitaka Ushiku, and Tatsuya Harada. Maximum classifier discrepancy for unsupervised domain adaptation. *CoRR*, abs/1712.02560, 2017.
- [77] Xinlei Chen and Kaiming He. Exploring simple siamese representation learning. In *Proceedings of the IEEE/CVF Conference on Computer Vision and Pattern Recognition*, pages 15750–15758, 2021.
- [78] Tatiana Tommasi, Novi Patricia, Barbara Caputo, and Tinne Tuytelaars. A deeper look at dataset bias. In *Domain adaptation in computer vision applications*, pages 37–55. Springer, 2017.
- [79] Boqing Gong, Fei Sha, and Kristen Grauman. Overcoming dataset bias: An unsupervised domain adaptation approach. In *NIPS Workshop on Large Scale Visual Recognition and Retrieval*, volume 3. Citeseer, 2012.
- [80] Paul S Bradley, Kristin P Bennett, and Ayhan Demiriz. Constrained K-means clustering. *Microsoft Research, Redmond*, 20(0):0, 2000.
- [81] Yuki Markus Asano, Christian Rupprecht, and Andrea Vedaldi. Self-labelling via simultaneous clustering and representation learning. *arXiv preprint arXiv:1911.05371*, 2019.

# A Prototype-Oriented Framework for Unsupervised Domain Adaptation: Appendix

Korawat Tanwisuth<sup>1</sup>, Xinjie Fan<sup>1</sup>, Huangjie Zheng<sup>1</sup>, Shujian Zhang<sup>1</sup>,  
Hao Zhang<sup>2</sup>, Bo Chen<sup>3</sup>, Mingyuan Zhou<sup>1</sup>

<sup>1</sup>The University of Texas at Austin   <sup>2</sup>Cornell University   <sup>3</sup>Xidian University

## A Broader impact

Any methods that deal with classification can suffer from dataset bias caused by domain shift between training and testing data. While domain adaptation can help mitigate the problem [78], it cannot eliminate the issue because of the combinatorial nature of too many exogenous factors [79]. Also, as with any computationally intensive endeavor, care must be taken to use sustainable energy sources. On a positive note, our method addresses many practical problems—including sampling variability, class-imbalance, and source-data privacy—by leveraging class prototypes.

## B EM steps derivation

Since the target label of each data point,  $y_j^t$ , is not observed, we can view it as a latent variable. The unknown quantity we are interested in is the proportion of classes in the target data  $p(\boldsymbol{\mu}_k) = p(y_j^t = k)$ . To infer this quantity, we maximize the likelihood on the observed target data:

$$l(\{p(\boldsymbol{\mu}_k)\}_{k=1}^K | \mathbf{x}_1^t, \mathbf{x}_2^t, \dots, \mathbf{x}_{n_t}^t) = \sum_{j=1}^{n_t} \ln \left[ \sum_{k=1}^K p(\boldsymbol{\mu}_k) p_{\boldsymbol{\theta}, \boldsymbol{\mu}}(\mathbf{x}_j | y_j^t = k) \right], \quad (9)$$

where  $p_{\boldsymbol{\theta}, \boldsymbol{\mu}}(\mathbf{x}_j | y_j^t = k) = \frac{\exp(\boldsymbol{\mu}_k^T \mathbf{f}_j^t)}{Z}$  and  $Z$  is a normalizing constant. Note that  $\boldsymbol{\mu}_k$  are learned jointly using the cross entropy loss on the source data.

Since it is difficult to directly optimize the marginal likelihood due to the sum inside the log function, we resort to the Expectation-Maximization (EM) algorithm, where we iterate between the expectation and maximization steps. We first initialize  $p(\boldsymbol{\mu}_k)$  with a uniform prior,  $p(\boldsymbol{\mu}_k)^0 = \frac{1}{K}$ ,  $\forall k = 1, 2, \dots, K$ , before performing the iterative updates. At each step  $l$  (starting from 0), we conduct the E-step and M-step as follows:

E-step: Compute the posterior probability of the target data belonging to class  $k$  using the old estimates. The posterior probabilities correspond to the weights of the transport cost of moving from target features to the prototypes.

$$p_{\boldsymbol{\theta}, \boldsymbol{\mu}}(y_j^t = k | \mathbf{x}_j^t, p(\boldsymbol{\mu}_k)^l) = \pi_{\boldsymbol{\theta}}(\boldsymbol{\mu}_k | \mathbf{f}_j^t, p(\boldsymbol{\mu}_k)^l) = \frac{p(\boldsymbol{\mu}_k)^l \exp(\boldsymbol{\mu}_k^T \mathbf{f}_j^t)}{\sum_{k'=1}^K p(\boldsymbol{\mu}_{k'})^l \exp(\boldsymbol{\mu}_{k'}^T \mathbf{f}_j^t)}$$

M-step: The log-likelihood of the complete data is given by  $\sum_{j=1}^{n_t} \ln [p(\boldsymbol{\mu}_k)^{l+1} p_{\boldsymbol{\theta}, \boldsymbol{\mu}}(\mathbf{x}_j | y_j^t)]$ . We maximize the expected complete log-likelihood where the expectation is taken with respect to the posterior distribution found in the E-step:

$$p(\boldsymbol{\mu}_k)^{l+1} = \operatorname{argmax}_{p(\boldsymbol{\mu}_k)^{l+1}} L \quad (10)$$

$$:= \operatorname{argmax}_{p(\boldsymbol{\mu}_k)^{l+1}} \sum_{j=1}^{n_t} \sum_{k=1}^K p_{\boldsymbol{\theta}, \boldsymbol{\mu}}(y_j^t = k | \mathbf{x}_j^t, p(\boldsymbol{\mu}_k)^l) \ln [p(\boldsymbol{\mu}_k)^{l+1} p_{\boldsymbol{\theta}, \boldsymbol{\mu}}(\mathbf{x}_j | y_j^t)] + \lambda \left( \sum_{k=1}^K p(\boldsymbol{\mu}_k)^{l+1} - 1 \right) \quad (11)$$



Here,  $\lambda$  is a Lagrange multiplier to enforce the constraint that  $p(\boldsymbol{\mu}_k)$  should lie in a simplex.

$$\frac{\partial L}{\partial \lambda} = \sum_{k=1}^K p(\boldsymbol{\mu}_k)^{l+1} - 1 = 0$$

$$\frac{\partial L}{\partial p(\boldsymbol{\mu}_k)^{l+1}} = \sum_{j=1}^{n_t} p_{\theta, \boldsymbol{\mu}}(y_j^t = k | \mathbf{x}_j^t, p(\boldsymbol{\mu}_k)^l) \frac{1}{p(\boldsymbol{\mu}_k)^{l+1}} + \lambda = 0$$

Multiplying both sides by  $p(\boldsymbol{\mu}_k)^{l+1}$  on and summing over  $k$ , we obtain the following update rule for  $p(\boldsymbol{\mu}_k)^{l+1}$ . And we get:

$$\lambda = -n_t,$$

$$p(\boldsymbol{\mu}_k)^{l+1} = \frac{1}{n_t} \sum_{j=1}^{n_t} p_{\theta, \boldsymbol{\mu}}(y_j^t = k | \mathbf{x}_j^t, p(\boldsymbol{\mu}_k)^l) = \frac{1}{n_t} \sum_{j=1}^{n_t} \pi(\boldsymbol{\mu}_k | \mathbf{f}_j^t, p(\boldsymbol{\mu}_k)^l).$$

In practice, we draw a mini-batch of size  $M$  to estimate this quantity.

## C Connection with K-means clustering and optimal transport

If we introduce a temperature parameter,  $\tau$ , fix the parameters of the feature encoder  $\theta$ , and let the negative pair-wise cost be the weighting function instead of the inner product, the conditional distribution becomes

$$\pi_{kj} := \pi_{\theta}(\boldsymbol{\mu}_k | \mathbf{f}_j^t) = \frac{p(\boldsymbol{\mu}_k) \exp\left(\frac{-c(\boldsymbol{\mu}_k, \mathbf{f}_j^t)}{\tau}\right)}{\sum_{k'=1}^K p(\boldsymbol{\mu}_{k'}) \exp\left(\frac{-c(\boldsymbol{\mu}_{k'}, \mathbf{f}_j^t)}{\tau}\right)}. \quad (12)$$

With a uniform prior and letting  $\tau \rightarrow 0$ , the conditional distribution becomes a one-hot encoding,  $\pi_{kj} = \mathbf{1}_{\{k = \operatorname{argmin}_{k'} c(\boldsymbol{\mu}_{k'}, \mathbf{f}_j^t)\}}$ , which is equivalent to solving the following constrained optimization problem:

$$\min_{\pi_{kj}} \frac{1}{M} \sum_{j=1}^M \sum_{k=1}^K \pi_{kj} c(\boldsymbol{\mu}_k, \mathbf{f}_j^t) \quad (13)$$

$$s.t. \quad \sum_{k=1}^K \pi_{kj} = 1, \quad \forall j, \quad (14)$$

$$\pi_{kj} \in \{0, 1\} \quad \forall j, k, \quad (15)$$

where  $\boldsymbol{\mu}_k$  is fixed. This is exactly the cluster assignment step in the K-Means clustering algorithm [80]. In other words, we assign each data point to its closest centroid. Thus, the update in the cross-entropy loss can be interpreted as the cluster-center update step and the update in the transport loss is analogous to the cluster assignment step.

As explained in the main text, we might not be able to rely on the cost,  $c(\boldsymbol{\mu}_k, \mathbf{f}_j^t)$ , alone because we do not have labels in the target domain. To avoid degenerate solutions, one might consider introducing a balanced constraint: each cluster should contain an equal number of data points. The constrained optimization problem then becomes:

$$\min_{\pi_{kj}} \frac{1}{M} \sum_{j=1}^M \sum_{k=1}^K \pi_{kj} c(\boldsymbol{\mu}_k, \mathbf{f}_j^t) \quad (16)$$

$$s.t. \quad \sum_{j=1}^M \pi_{kj} = \frac{M}{K}, \quad \forall k \quad (17)$$

$$\pi_{kj} \in \{0, 1\}, \quad \forall k. \quad (18)$$

This is an integer programming problem and may look difficult to optimize. However, one can relax the decision variables,  $\pi_{kj}$ , to be continuous and solve the following constrained optimization problem instead:

$$\min_{\pi_{kj}} \frac{1}{M} \sum_{j=1}^M \sum_{k=1}^K \pi_{kj} c(\boldsymbol{\mu}_k, \mathbf{f}_j^t) \quad (19)$$

$$s.t. \quad \sum_{j=1}^M \pi_{kj} = \frac{1}{K}, \quad \forall k \quad (20)$$

$$\sum_{k=1}^K \pi_{kj} = \frac{1}{M}, \quad \forall j \quad (21)$$

$$\pi_{kj} \geq 0, \quad \forall j, k. \quad (22)$$

The formulation above is the optimal transport problem discussed in the text where the marginal constraints are uniform distributions over data points and classes. While we are solving a continuous relaxation of the integer programming problem, solving this problem leads to an integral solution [81], meaning that the optimal transport problem is equivalent to the cluster assignment step of the K-means algorithm with a balanced constraint. Note that the statement holds when  $M$  is divisible by  $K$ .

## D Implementation details

We implement our method on top of the open-source transfer learning library (MIT license) [66], adopting the default neural network architectures for both the feature encoder and linear classifier. For the feature encoder network, we utilize a pre-trained ResNet-50 in all experiments except for multi-source domain adaptation, where we use a pre-trained ResNet-101. We fine-tune the feature encoder and train the linear layers from random initialization. The linear layers have the learning rate of 0.01, ten times that of the feature encoder. The learning rate follows the following schedule:  $\eta_{\text{iter}} = \eta_0(1 + \gamma \text{iter})^{-\alpha}$ , where  $\eta_0$  is the initial learning rate. We set  $\eta_0$  to 0.01,  $\gamma$  to 0.0002, and  $\alpha$  to 0.75. We utilize a mini-batch SGD with a momentum of 0.9. We set the batch size for the source data as  $N = 32$  and that for the target data as  $M = 96$ . We use all the labeled source samples and unlabeled target samples [6, 7, 26]. We set  $\beta_0$  to 0 (using a uniform prior) in all settings except for the sub-sampled target datasets. We perform a sensitivity analysis (see Appendix E) and set  $\beta_0$  empirically to 0.001 for the sub-sampled target version of Office-31 and 0.0001 for that of Office-Home. We report the average accuracy from three independent runs. All experiments are conducted using a single Nvidia Tesla V100 GPU except for the DomainNet experiment, where we use four V100 GPUs.

In both the single and multi-source settings, we set  $\beta_0 = 0$ , which corresponds to using a uniform prior. We do not perform any additional hyper-parameter searches. The cross-entropy and transport losses are equally weighted. We run each experiment for 10,000 iterations for the single-source setting. For the multi-source setting, we train the model for 75,000 iterations.

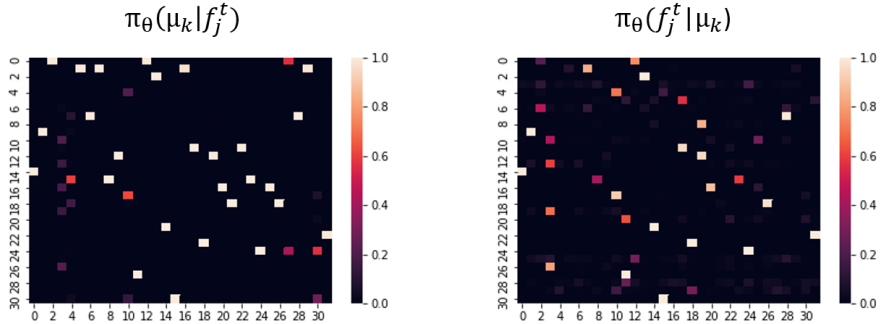
In the class imbalance setting, we follow the experimental protocol in Tachet des Combes et al. [18] and quote the results directly when available. We perform a sensitivity analysis on the parameter,  $\beta_0$ , and present the result in Table 8. In the sub-sampled target datasets, we empirically set  $\beta_0$  to 0.001 for Office-31 and 0.0001 for Office-Home. For sub-sampled source datasets, we set  $\beta_0$  to 0 in all experiments. In all of the above settings, we run three independent experiments using the seeds  $\{0, 1, 2\}$ .

In the source-private domain adaptation setting, we implement our method using the same setup as Liang et al. [31]. We use all the same hyper-parameters except for the maximum number of epochs and target batch size. We set the number of epochs to 70 for Office-31 and 100 for Office-Home. The target batch size is set to 96. We change the two parameters to adjust for the number of data seen since SHOT goes through the whole training set at every 15 iterations. We use the same random seeds,  $\{2019, 2020, 2021\}$ , as the original paper.

## E Additional experimental results

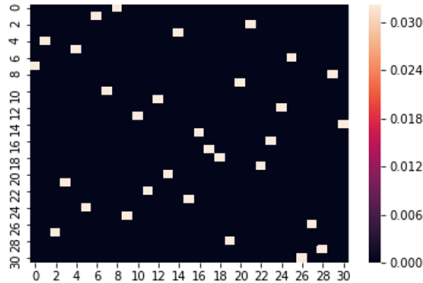
**Details on the synthetic experiment (Figure 2).** In this experiment, we provide an illustration of our method as well as the baseline, DANN, on a toy dataset. We sample two dimensional data from multivariate Gaussian distributions with different means but the same covariance matrix,  $\Sigma = \begin{bmatrix} 0.5 & -0.3 \\ -0.3 & 0.5 \end{bmatrix}$ . In each domain, we draw 300 examples. We draw 250 of the green class from  $\mathcal{N}([7, 5.5], \Sigma)$  and 50 of the red class from  $\mathcal{N}([4, 3.5], \Sigma)$ . In the target domain, we draw 50 of the green class from  $\mathcal{N}([7.5, 3.5], \Sigma)$  and 250 of the red class from  $\mathcal{N}([4.4, 5], \Sigma)$ . We utilize a three-layer feature encoder with hidden dimension 15 and output dimension 2 to visualize the latent space. The classifier is a linear layer.

**Visualization of transport probabilities.** In Figure 5, we visualize transport probabilities on a sample batch of data for PCT and POT. As explained earlier, OT is equivalent to solving a balanced-constrain K-means when  $M$  is divisible by  $K$  so we set  $M = K = 31$ . In Figure 5b, we can see that OT gives equal weight to all the assigned points, and each row (class) contains only one active cell, meaning that each data point is assigned into a distinct cluster. In Figure 5a, the active cells in  $\pi_{\theta}(\mu_k | f_j^t)$  usually correspond to those in  $\pi_{\theta}(f_j^t | \mu_k)$ . However, the magnitudes often differ:  $\pi_{\theta}(\mu_k | f_j^t)$  takes into account the uncertainty in the classes whereas  $\pi_{\theta}(f_j^t | \mu_k)$  considers the uncertainty of the target features.  $\pi_{\theta}(\mu_k | f_j^t)$  will have at least one active cell across the rows (every data point is close to some prototype), while  $\pi_{\theta}(f_j^t | \mu_k)$  will have at least one active cell across the columns (every prototype is close to some target feature).



(a)

*OT plan*



(b)

Figure 5: Visualization of transport probabilities for PCT and POT. The rows correspond to different  $\mu_k$  whereas the columns correspond to different  $f_j^t$ .

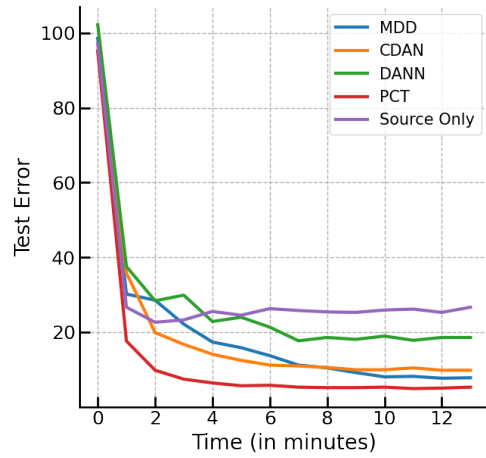


Figure 6: Test error vs. training time in minutes for different algorithms trained on the task  $A \rightarrow W$ .

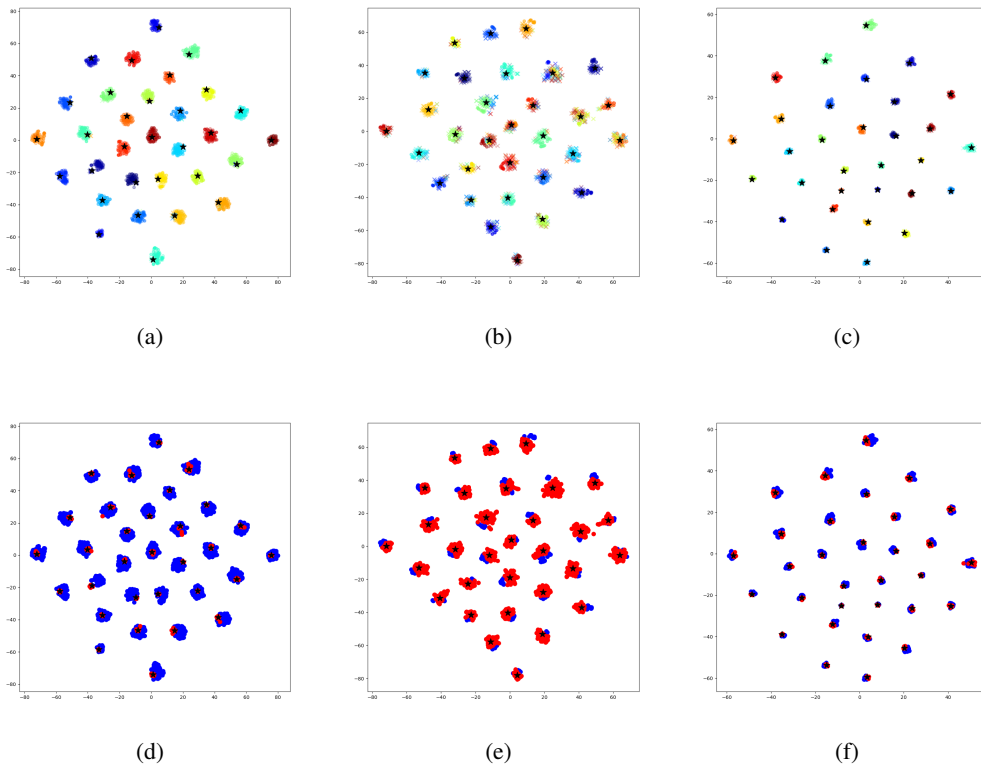


Figure 7: TSNE visualizations on the Office-31 dataset. The plots in each column correspond to each transfer task: (a),(d) to  $A \rightarrow D$ , (b),(e) to  $D \rightarrow A$ , and (c),(f) to  $W \rightarrow D$ . Plots in the top row highlight class information whereas those in the bottom row exhibit domain information. In the top row, each plot shows that both the source (dots  $\cdot$ ) and target (crosses  $\times$ ) features are close to the prototypes (black stars  $\star$ ). In the bottom row, we can see that the blue dots (source domain) are close to the red dots (target domain).

**Sensitivity analysis.** In Table 8, we can see that  $\beta_0$  works well in the range of 0.0001 – 0.01. Generally,  $\beta_0$  should be set to a small value because the average predictions of a single mini-batch can be noisy. Thus, we give more weight to the weighted sum of the past average predictions over multiple mini-batches, which are more stable.

Table 8: Accuracy (%) on the task (A→ sW) for the sub-sampled (target) Office-31 for different values of  $\beta_0$  (ResNet-50).

$\beta_0$	1	0.1	0.01	0.001	0.0001	0
	37.8	80.2	88.5	<b>88.9</b>	88.5	87.2

## E.1 Full experimental results

Due to space constraints, we report the average accuracy of different transfer tasks of a dataset in some experiments. Below, we present the full tables, which include the average accuracy of the individual tasks.

### E.1.1 Ablation study

Table 9: Accuracy (%) of PCT on Office-31 under different variants (ResNet-50).

Method	A → W	D → W	W → D	A → D	D → A	W → A	Avg
PCT w/o ( $\mathcal{L}_{t \rightarrow \mu}$ )	92.7	98.1	99.8	92.0	75.3	73.6	88.6
PCT w/o ( $\mathcal{L}_{\mu \rightarrow t}$ )	84.4	98.5	99.9	89.8	69.0	64.0	84.3
POT	94.1	97.6	97.8	89.7	74.0	74.1	87.9
POT-Sinkhorn	94.4	98.1	98.3	89.6	75.3	74.0	88.3
w/o stop-grad $\mu$	92.4	98.8	<b>100.0</b>	93.4	75.8	73.8	89.0
$c(\mu_k, \mathbf{f}_j^t) = \exp(-\mu_k^T \mathbf{f}_j^t)$	90.4	<b>98.9</b>	<b>100.0</b>	89.9	72.8	69.5	86.9
PCT (Ours)	<b>94.6 ± 0.5</b>	98.7 ± 0.4	99.9 ± 0.1	<b>93.8 ± 1.8</b>	<b>77.2 ± 0.5</b>	<b>76.0 ± 0.9</b>	<b>90.0</b>

### E.1.2 Sub-sampled setting

Table 10: Accuracy (%) on the sub-sampled (source) Office-31 for unsupervised domain adaptation (ResNet-50).

Method	sA → W	sD → W	sW → D	sA → D	sD → A	sW → A	Avg
ResNet-50	70.7	95.3	97.3	75.8	56.8	58.4	75.7
DANN	77.7	93.8	96.0	75.5	56.6	57.5	76.2
JAN	77.6	91.7	92.6	77.8	64.5	65.1	78.2
CDAN	84.6	96.8	98.3	82.5	62.5	65.0	81.6
IWDANN	88.4	97.0	98.7	81.6	65.0	64.9	82.6
IWJAN	83.3	96.3	98.8	84.6	65.3	67.4	82.6
IWCDAN	87.3	97.7	99.0	86.6	66.5	66.3	83.9
PCT-Uniform (Ours)	<b>92.4 ± 1.2</b>	<b>97.8 ± 0.4</b>	<b>99.4 ± 0.0</b>	<b>91.1 ± 2.2</b>	<b>73.9 ± 0.5</b>	<b>73.0 ± 1.1</b>	<b>87.9</b>

Table 11: Accuracy (%) on the sub-sampled (target) Office-31 for unsupervised domain adaptation (ResNet-50).

Method	A → sW	D → sW	W → sD	A → sD	D → sA	W → sA	Avg
ResNet-50	68.4	96.7	99.3	68.9	62.5	60.7	76.1
DANN	76.3	88.0	93.0	72.9	62.3	63.1	75.9
JAN	78.5	89	92.1	81.4	62.9	64.9	78.1
CDAN	85.8	97.6	99.9	85.2	64.9	64.6	83.0
IWDANN	76.4	97.1	<b>100.0</b>	82.7	59.0	59.9	79.2
IWJAN	83.6	97.9	99.7	86.2	64.0	65.6	82.8
IWCDAN	87.9	97.7	<b>100.0</b>	86.2	64.8	64.1	83.5
PCT-Uniform (Ours)	86.4 ± 0.86	97.3 ± 0.3	<b>100.0 ± 0.5</b>	88.5 ± 0.8	69.5 ± 0.9	70.5 ± 0.7	85.4
PCT-Learnable (Ours)	<b>88.1 ± 0.5</b>	<b>98.5 ± 0.4</b>	99.9 ± 0.17	<b>90.4 ± 1.7</b>	<b>69.9 ± 0.37</b>	<b>71.3 ± 0.51</b>	<b>86.4</b>

Table 12: Accuracy (%) on the sub-sampled (source) Office-Home for unsupervised domain adaptation (ResNet-50).

Method	sAr → Cl	sAr → Pr	sAr → Rw	sCl → Ar	sCl → Pr	sCl → Rw	sPr → Ar	sPr → Cl	sPr → Rw	sRw → Ar	sRw → Cl	sRw → Pr	Avg
ResNet-50	35.7	54.7	62.6	43.7	52.5	56.6	44.3	33.0	65.2	57.1	40.5	70.0	51.4
DANN	36.1	54.2	61.7	44.3	52.6	56.4	44.6	37.1	65.2	56.7	43.2	69.9	51.8
JAN	34.5	56.9	64.5	46.2	56.8	59.0	50.6	37.2	70.0	58.7	40.6	72.00	53.9
CDAN	38.9	56.8	64.8	48.0	60.0	61.2	49.7	41.4	70.2	62.4	47.0	74.7	56.3
IWDANN	39.8	63.0	68.7	47.4	61.1	60.4	50.4	41.6	72.5	61.0	49.4	76.1	57.6
IWJAN	36.2	61.0	66.3	48.7	59.9	61.9	52.9	37.7	70.9	60.3	41.5	73.3	55.9
IWCDAN	43.0	65.0	71.3	52.9	64.7	66.5	54.9	44.8	75.9	67.0	50.5	78.6	61.2
PCTUniform (Ours)	<b>51.9 ± 0.2</b>	<b>69.7 ± 0.9</b>	<b>76.5 ± 0.3</b>	<b>63.3 ± 1.3</b>	<b>70.8 ± 0.4</b>	<b>71.1 ± 0.5</b>	<b>66.0 ± 0.8</b>	<b>49.9 ± 0.7</b>	<b>80.2 ± 0.5</b>	<b>73.1 ± 0.6</b>	<b>58.6 ± 0.7</b>	<b>83.2 ± 0.8</b>	<b>67.8</b>

Table 13: Accuracy (%) on the sub-sampled (target) Office-Home for unsupervised domain adaptation (ResNet-50).

Method	Ar → sCl	Ar → sPr	Ar → sRw	Cl → sAr	Cl → sPr	Cl → sRw	Pr → sAr	Pr → sCl	Pr → sRw	Rw → sAr	Rw → sCl	Rw → sPr	Avg
ResNet-50	41.5	65.8	73.6	52.2	59.5	63.6	51.5	36.4	71.3	65.2	42.8	75.4	58.2
DANN	47.8	55.9	66.0	45.3	54.8	56.8	49.4	48.0	70.2	65.4	55.5	72.7	58.3
JAN	45.8	69.7	74.9	53.9	63.2	65.0	56	42.5	74	65.9	47.4	78.8	61.4
CDAN	51.1	69.7	74.6	56.9	60.4	64.6	57.2	45.5	75.6	68.5	52.7	79.8	63.0
IWDANN	48.7	62.0	71.6	50.4	57.0	60.3	51.4	41.1	69.9	62.6	51.0	77.2	58.6
IWJAN	44.0	71.9	75.1	55.2	65.0	67.7	57.1	42.4	74.9	66.1	46.1	78.5	62.0
IWCDAN	52.3	72.2	76.3	56.9	67.3	67.7	57.2	46.0	77.8	67.3	53.8	80.6	64.6
PCT-Uniform (Ours)	55.8 ± 0.5	77.6 ± 0.6	80.4 ± 0.3	65.1 ± 1.2	72.3 ± 2.0	74.7 ± 0.2	<b>67.0 ± 1.5</b>	<b>50.9 ± 1.0</b>	81.1 ± 0.3	72.6 ± 0.2	57.0 ± 0.2	<b>84.0 ± 0.2</b>	69.8
PCT-Learnable (Ours)	<b>57.5 ± 0.4</b>	<b>78.2 ± 0.2</b>	<b>80.5 ± 0.0</b>	<b>66.7 ± 0.6</b>	<b>74.3 ± 1.3</b>	<b>75.4 ± 0.5</b>	64.6 ± 1.5	50.7 ± 1.4	<b>81.3 ± 0.4</b>	<b>72.9 ± 0.3</b>	<b>57.3 ± 0.9</b>	83.5 ± 0.15	<b>70.2</b>

### E.1.3 Source-private setting

Table 14: Accuracy (%) on the source-private Office-31 for unsupervised domain adaptation (ResNet-50).

Method	A → W	D → W	W → D	A → D	D → A	W → A	Avg
Source Model Only	76.8	95.3	98.7	80.8	60.3	63.6	79.3
SHOT-Pseudo-Label	90.8	96.6	99.3	93.2	72.1	73.5	87.6
SHOT-IM	91.2	98.3	99.9	90.6	72.5	71.4	87.3
SHOT	90.1	<b>98.4</b>	<b>99.9</b>	<b>94.0</b>	<b>74.7</b>	74.3	<b>88.6</b>
PCT (Ours)	<b>91.7 ± 0.8</b>	97.9 ± 0.3	<b>99.9 ± 0.2</b>	92.2 ± 1.1	74.0 ± 1.6	<b>74.6 ± 0.3</b>	88.4

Table 15: Accuracy (%) on the source-private Office-Home for unsupervised domain adaptation (ResNet-50).

Method	Ar → Cl	Ar → Pr	Ar → Rw	Cl → Ar	Cl → Pr	Cl → Rw	Pr → Ar	Pr → Cl	Pr → Rw	Rw → Ar	Rw → Cl	Rw → Pr	Avg
ResNet-50	44.6	67.3	74.8	52.7	62.7	64.8	53.0	40.6	73.2	65.3	45.4	78.0	60.2
SHOT	57.1	78.1	81.5	68.0	<b>78.2</b>	<b>78.1</b>	<b>67.4</b>	54.9	<b>82.2</b>	73.3	58.8	<b>84.3</b>	<b>71.8</b>
PCT (Ours)	56.6 ± 1.1	77.0 ± 0.6	79.8 ± 0.5	<b>68.3 ± 0.5</b>	75.7 ± 0.4	75.5 ± 0.3	67.3 ± 1.3	<b>55.1 ± 1.0</b>	80.2 ± 0.9	<b>74.4 ± 0.5</b>	<b>58.9 ± 0.5</b>	83.2 ± 0.7	71.0

## E.2 Additional Results

To further verify the efficacy of our framework, we provide additional results on the Cross-Digits, Office-Caltech, Image-Clef, and VisDA under different settings.

### E.2.1 Single-source setting

Table 16: Average Accuracy (%) on the Cross-Digits dataset for unsupervised domain adaptation (ResNet-50).

Method	MNIST → USPS	SVHN → MNIST	USPS → MNIST	Avg
CDAN	95.6	89.2	<b>98.0</b>	94.3
rRevGrad+CAT	94	98.8	96	96.3
ETD	96.4	97.9	96.3	96.9
PCT (Ours)	<b>97.8 ± 0.1</b>	<b>98.9 ± 0.0</b>	97.0 ± 0.6	<b>98.0</b>

Table 17: Average Accuracy (%) on the Office-Caltech dataset for unsupervised domain adaptation (ResNet-50).

Method	A → W	A → D	A → C	D → A	D → W	D → C	W → A	W → D	W → C	C → A	C → W	C → D	Avg
CDAN	<b>99.3</b>	96.8	95.4	94.7	<b>100.0</b>	94.6	95.7	<b>100.0</b>	94.5	94.8	95.9	92.4	96.2
MDD	98.3	98.0	94.8	95.3	98.6	94.3	95.6	<b>100.0</b>	94.9	<b>95.8</b>	96.3	<b>98.7</b>	96.7
PCT (Ours)	99.1 ± 0.1	<b>98.5 ± 0.3</b>	<b>95.6 ± 0.1</b>	<b>96.3 ± 0.3</b>	99.8 ± 0.17	<b>95.1 ± 0.3</b>	<b>96.2 ± 0.1</b>	<b>100 ± 0.0</b>	<b>95.2 ± 0.2</b>	<b>95.8 ± 0.4</b>	<b>98.7 ± 0.4</b>	96.6 ± 1.0	<b>97.3</b>

Table 18: Average Accuracy (%) on the Image-Clef dataset for unsupervised domain adaptation (ResNet-50).

Method	I → P	P → I	I → C	C → I	C → P	P → C	Avg
CDAN	77.7	90.7	97.7	91.3	74.2	94.3	87.7
rRevGrad+CAT	77.2	91	95.5	91.3	75.3	93.6	87.3
ETD	<b>81</b>	91.7	<b>97.9</b>	<b>93.3</b>	<b>79.5</b>	95	<b>89.7</b>
PCT (Ours)	78.5 ± 0.4	<b>93.1 ± 0.2</b>	97.0 ± 0.3	92.2 ± 0.2	75.7 ± 0.6	<b>95.4 ± 0.4</b>	88.7

## E.2.2 Multi-source setting

Table 19: Average Accuracy (%) on the Office-31 dataset for ResNet50-based MSDA methods.

Category	Method	$\mathcal{R} \rightarrow D$	$\mathcal{R} \rightarrow W$	$\mathcal{R} \rightarrow A$	Avg
Multi-source	DCTN	99.3	98.2	64.2	87.2
	MFSAN	99.5	<b>98.5</b>	72.7	90.2
	SImpAI	99.2	97.4	70.6	89.0
Source-combined	DAN	99.6	97.8	67.6	88.3
	D-CORAL	99.3	98.0	67.1	88.1
	RevGrad	99.7	98.1	67.6	88.5
	PCT (Ours)	<b>99.8 ± 0.0</b>	<b>98.5 ± 0.1</b>	<b>76.9 ± 0.6</b>	<b>91.7</b>

## E.2.3 Source-private setting

Table 20: Accuracy (%) on the VisDA-2017 dataset for unsupervised domain adaptation (ResNet-50).

ETN	STA	UAN	DANCE	PCT (Ours)
64.1	48.1	66.4	70.2	<b>71.2 ± 0.8</b>